iScience

CellPress
OPEN ACCESS

Article

Targeting Bcl-xL is a potential therapeutic strategy for extranodal NK/T cell lymphoma

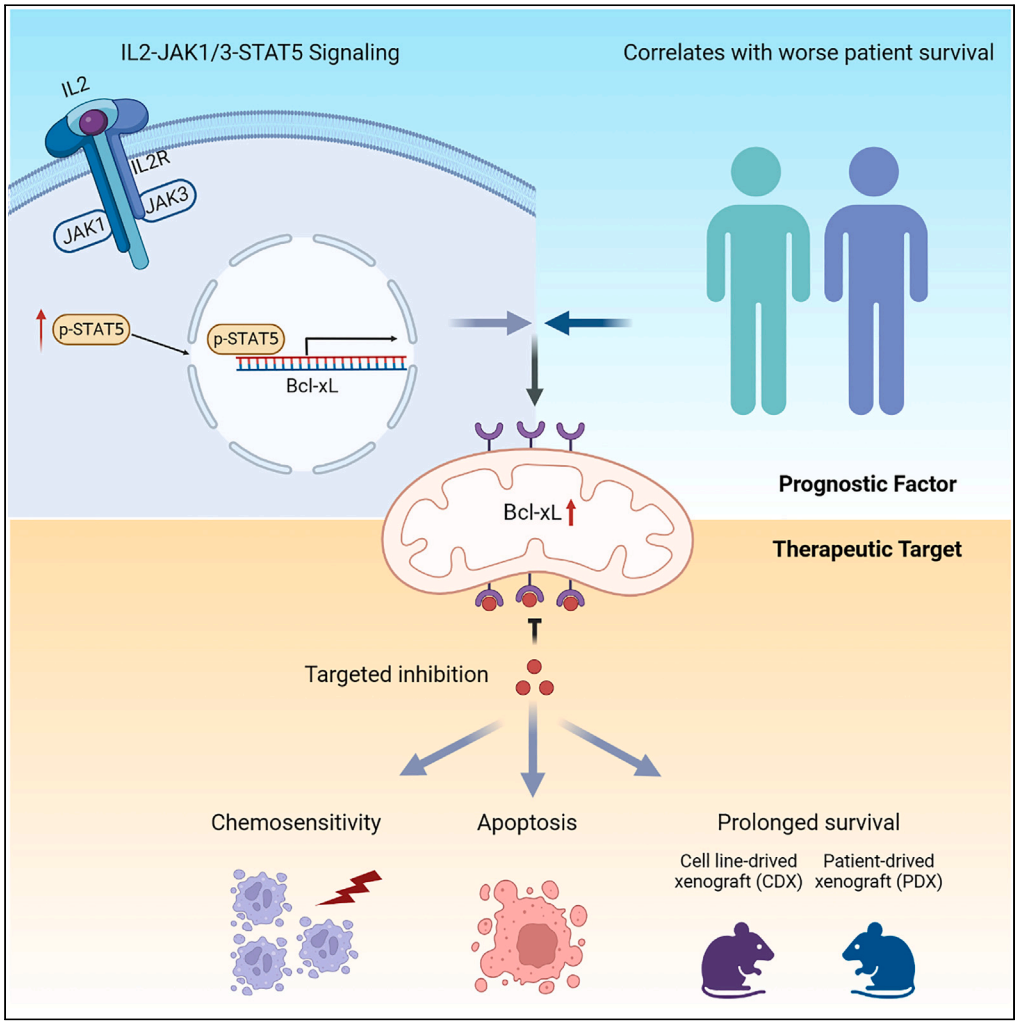

Chuanxu Liu, Xinyu Ding, Gaoyang Li, ..., Biao Jiang, Qianqian Yin, Rong Tao

jiangbiao@shanghaitech.edu.cn (B.J.)
yinqq@shanghaitech.edu.cn (Q.Y.)
rtao@shca.org.cn (R.T.)

Highlights

Bcl-xL is specifically upregulated in ENKTL

Bcl-xL high expression is closely associated with worse patient survival

IL2-JAK1/3-STAT5 signaling pathway is involved in Bcl-xL dysregulation

Targeted inhibition of Bcl-xL exhibits therapeutic benefits *in vitro* and *in vivo*

Liu et al., iScience 26, 107369
August 18, 2023
https://doi.org/10.1016/j.isci.2023.107369

iScience

CellPress
OPEN ACCESS

Article

Targeting Bcl-xL is a potential therapeutic strategy for extranodal NK/T cell lymphoma

Chuanxu Liu,[1,3,8] Xinyu Ding,[2,8] Gaoyang Li,[2,8] Youping Zhang,[3] Yubao Shao,[2] Linyi Liu,[2] Wenhao Zhang,[1,3] Yujie Ma,[3] Wenbin Guan,[4] Lifeng Wang,[4] Zhongli Xu,[2] YungTing Chang,[5] Yongqiang Zhang,[6] Biao Jiang,[2,7,*] Qianqian Yin,[2,9,*] and Rong Tao[1,3,*]

SUMMARY

Extranodal natural killer/T cell lymphoma, nasal type (ENKTL) is an aggressive lymphoid malignancy with a poor prognosis and lacks standard treatment. Targeted therapies are urgently needed. Here we systematically investigated the druggable mechanisms through chemogenomic screening and identified that Bcl-xL-specific BH3 mimetics effectively induced ENKTL cell apoptosis. Notably, the specific accumulation of Bcl-xL, but not other Bcl-2 family members, was verified in ENKTL cell lines and patient tissues. Furthermore, Bcl-xL high expression was shown to be closely associated with worse patient survival. The critical role of Bcl-xL in ENKTL cell survival was demonstrated utilizing selective inhibitors, genetic silencing, and a specific degrader. Additionally, the IL2-JAK1/3-STAT5 signaling was implicated in Bcl-xL dysregulation. *In vivo*, Bcl-xL inhibition reduced tumor burden, increased apoptosis, and prolonged survival in ENKTL cell line xenograft and patient-derived xenograft models. Our study indicates Bcl-xL as a promising therapeutic target for ENKTL, warranting monitoring in ongoing clinical trials by targeting Bcl-xL.

INTRODUCTION

Extranodal natural killer/T cell lymphoma, nasal type (ENKTL), is an aggressive and heterogeneous malignancy of non-Hodgkin's lymphoma with a poor prognosis.[1,2] It shows a strong association with Epstein-Barr virus (EBV) infection with a type II latency pattern, which is much more prevalent in Asia and Latin America than in Western countries.[3] For the current ENKTL treatment, asparaginase-containing regimens,such as SMILE (dexamethasone, methotrexate, ifosfamide, L-asparaginase, and etoposide), GELAD (gemcitabine, etoposide, pegaspargase, and dexamethasone), DDGP (dexamethasone, cisplatin, gemcitabline, and pegaspargase), and MEDA (methotrexate, etoposide, dexamethasone, and pegaspargase), evolve from anthracycline-based chemotherapy, such as CHOP(cyclophosphamide, doxorubicin, vincristine and prednisone), and offer superior benefits for ENKTL patients.[4–7] However, the standard therapy strategies have not yet been established, and the prognosis of patients refractory to the asparaginase-based option or experiencing a relapse or recurrence remains very poor with the current chemotherapy and radiotherapy treatment.[8,9] Therefore, further investigations are required to improve the understanding of the pathogenesis and therapeutics of ENKTL.

Multi-omics analysis utilizing techniques such as whole-genome sequencing and gene expression profiling has been performed to reveal alterations of genetics, epigenetics, and signaling pathways potentially involved in the pathogenesis of ENKTL.[10,11] Recurrent genomic aberrations have been identified in ENKTL, for example, the chromosome 6q region deletion and somatic mutations such as DDX3X, TP53, BCOR, JAK3, STAT, and ECSIT.[11] Besides, aberrant signaling pathways that are frequently activated in ENKTL, such as the Janus-associated kinase/signal transducer and activator of transcription (JAK/STAT) and nuclear factor kappa B (NF-κB) signaling pathways, have been uncovered to be potential therapeutic targets.[1,12] In addition, immune evasion mediated by the upregulation of programmed cell death ligand 1 (PDL1) has been revealed as an important mechanism for ENKTL survival.[13] However, ENKTL pathogenesis, especially the therapy resistance mechanism of ENKTL, is still poorly understood, and continued investigations are needed to identify critical genetic drivers of this disease.

The B cell lymphoma-2 (Bcl-2) family proteins are central regulators of apoptosis triggered by multiple stimulations and stress signals, which comprise anti-apoptotic members including Bcl-2, Bcl-xL (BCL2L1), Mcl-1,

[1]Department of Lymphoma, Fudan University Shanghai Cancer Center, Shanghai 200032, China

[2]Shanghai Institute for Advanced Immunochemical Studies, School of Life Science and Technology, ShanghaiTech University, Shanghai 201210, China

[3]Department of Hematology, Xinhua Hospital, Shanghai Jiao Tong University School of Medicine, Shanghai 200092, China

[4]Department of Pathology, Xinhua Hospital of Shanghai Jiao Tong University School of Medicine, Shanghai 200092, China

[5]Department of Pharmacy, Renji Hospital, Shanghai Jiao Tong University School of Medicine, Shanghai 200127, China

[6]State Key Laboratory of Bioengineering Reactor, Shanghai Key Laboratory of New Drug Design and School of Pharmacy, East China University of Science and Technology, Shanghai 200237, China

[7]CAS Key Laboratory of Synthetic Chemistry of Natural Substances, Shanghai Institute of Organic Chemistry, Chinese Academy of Sciences, Shanghai 200032, China

[8]These authors contributed equally

[9]Lead contact

*Correspondence: jiangbiao@shanghaitech.edu.cn (B.J.), yinqq@shanghaitech.edu.cn (Q.Y.), rtao@shca.org.cn (R.T.)

https://doi.org/10.1016/j.isci.2023.107369

BFL1 (BCL2A1), and BCL-W (BCL2L2), pro-apoptotic effectors (BAK and BAX), and pro-apoptotic BH3-only activators such as BIM (BCL2L11) and BID.[14] As a key hallmark of cancer, the evasion of apoptosis is involved in tumor development and treatment resistance, which is at least partially attributable to the aberrant expression of the anti-apoptotic Bcl-2 family members.[15,16] Therefore, the inhibitors of anti-apoptotic Bcl-2 family members, especially with BH3 mimetics, have been extensively investigated as therapeutic options for cancer.[17] Bcl-xL is a well-defined pro-survival protein with the broadest spectrum of pro-apoptotic counterparts. The predominant overexpression of Bcl-xL is correlated with disease progression and clinical therapy resistance in a variety of solid tumors and a subset of leukemia cells.[18–20] It underscores the potential application of Bcl-xL inhibitors in cancer cells addicted to Bcl-xL.

Here we performed high-throughput chemogenomic screening using a targeted chemical library of small molecules with known drug targets and identified Bcl-xL as a critical survival factor in ENKTL. We demonstrated the specific accumulation of Bcl-xL in ENKTL cell lines and patient tissues, and tumor-specific overexpression of Bcl-xL is closely associated with poorer overall survival (OS) of ENKTL patients. We deciphered the molecular basis underlying Bcl-xL upregulation associated with the interleukin-2 (IL-2)-JAK1/3-STAT5 signaling pathway. Moreover, the therapeutic benefits of Bcl-xL inhibition *in vivo* were investigated in the ENKTL cell line-derived xenograft (CDX) model and patient-derived xenograft (PDX) murine models. Collectively, Bcl-xL is identified as a critical pro-survival factor of ENKTL *in vitro* and *in vivo*, and targeting the Bcl-xL alone or in combination with clinical chemotherapy drugs could be a promising therapeutic strategy applied to this disease. Our preclinical results indicate that Bcl-xL is a promising therapeutic target in ENKTL and insight into conducting clinical translational research by targeting Bcl-xL (www.clinicaltrials.gov; #NCT05186012).

RESULTS

A chemogenomic screening identifies Bcl-xL as a potential target for ENKTL

To identify potential therapeutic targets and druggable mechanisms of ENKTL, we performed a high-throughput cell viability screen in the ENKTL cell line SNK-6 cells[21] with a chemogenomic library, including the U.S. Food and Drug Administration (FDA)-approved drugs and bioactive inhibitors with known drug targets (2,076 compounds) (Figure 1A and Table S1). In the primary screen in SNK-6 cells, 117 candidates achieved more than 50% growth inhibition at the tested concentration (1 μM). These candidates were further selected to perform the second-round screen using the same test concentrations in two other ENKTL cell lines, SNK-1 and SNT-8.[21,22] Finally, cytotoxic drugs were excluded, and 60 small-molecule compounds with known targets were obtained for further target analysis (Figure 1B). BH3-mimetic drugs, including a Bcl-xL/Bcl-2 dual inhibitor-Navitoclax (ABT-263) and its predecessor ABT-737, as well as two Bcl-xL-specific inhibitors A-1331852 (A-133) and A-1155463 (A-115),[16] were identified as the strong candidates for effective ENKTL cell killing (Figure 1C). In contrast, specific Bcl-2 inhibitors such as ABT-199[23] did not show activity in the screening, further suggesting the vital role of Bcl-xL in ENKTL cells.

To explore whether the sensitivity of BH3 mimetics targeting Bcl-xL is closely associated with aberrant Bcl-xL expression in ENKTL, the levels of Bcl-xL and other Bcl-2 family members were studied in ENKTL cell lines and control cells, including normal peripheral blood mononuclear cells (PBMCs) from healthy adult donors, purified $CD56^+$ population from normal PBMCs, and immortalized cell lines as well as a panel of cancer cell lines derived from hematologic malignancies and solid tumors. It is worth mentioning that we established a new ENKTL cell line designated LY cells and demonstrated its cell morphology, cell-surface marker analysis by flow cytometry, and short tandem repeat (STR) analysis (Figures S1A–S1C. Please also see STAR methods for more details). In addition to the three ENKTL cell lines utilized above (SNK-1, SNK-6, and SNT-8 cells), LY cells were also included in our study. Markedly, our data demonstrated that Bcl-xL was specifically accumulated at much higher levels in all ENKTL cell lines compared with that of PBMCs and purified $CD56^+$ natural killer (NK) population from healthy individuals (Figure 1D). Besides, the significant upregulation of Bcl-xL at both mRNA level (Figure 1E) and protein level (Figures 1F and 1G) was also observed in all ENKTL cell lines compared with normal PBMCs, non-tumorigenic cells, and other types of cancer cell lines. On the contrary, the expression patterns of other Bcl-2 family members did not exert specific dysregulation in ENKTL cell lines except for BFL1, which was significantly decreased at the mRNA level compared with that of normal PBMCs (Figures S2A–S2D). Of note, studies have shown that Bcl-xL expression was elevated in several solid tumor cell lines, such as nasopharyngeal carcinoma cell lines (NPCs) and a subset of leukemia cell lines (e.g., Molt-4), but Bcl-xL is much more highly expressed in ENKTL cell lines, further suggesting the relevance of Bcl-xL overexpression and ENKTL pathogenesis.

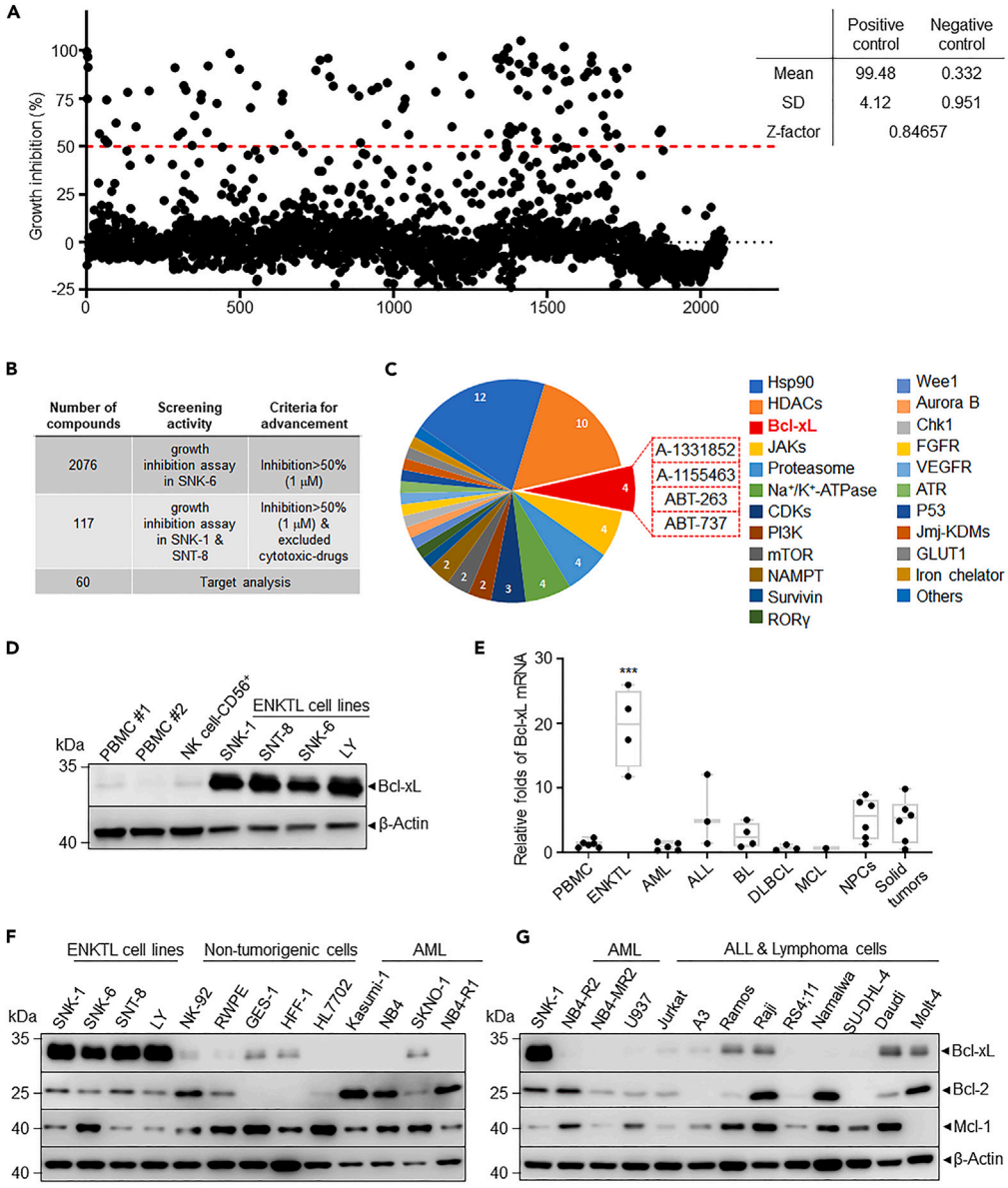

Figure 1. A high-throughput drug screen identifies aberrant anti-apoptosis pathways in ENKTL

(A) SNK-6 cells were seeded in 384-well plates and treated with bioactive chemogenomic library (1 μM) in the primary drug screen. Scatterplot of the growth inhibitory rate (%) of all the compounds normalized to the negative control wells (0.1% DMSO treatment). The dashed line represents 50% growth inhibition rate.

(B) An outline of the drug-screening procedure. 117 candidates (the growth inhibition rate >50% in SNK-6) were validated in SNK-1 and SNT-8 cells for secondary screening.

(C) Target analysis of 60 final candidate compounds. The numbers in the sector diagram show the number of compounds within each category. "Hits" highlighted in red are compounds that are inhibitors of Bcl-xL.

(D and E) The level of protein (D) and mRNA (E) of Bcl-xL were detected by western blots and quantitative real-time PCR, respectively. $p < 0.001$ (***) was determined by one-way ANOVA analysis. AML, acute myeloid leukemia; ALL, acute lymphocytic leukemia; BL, burkitt lymphoma; DLBCL, diffuse large B cell lymphoma; MCL, mantle cell lymphoma; NPC, nasopharyngeal carcinoma. Error bars represent the mean ± SD in an independent experiment, n = 6 for PBMC, NPCs and solid tumors, n = 5 for AML, n = 4 for ENKTL and BL, n = 3 for ALL and DLBCL.

(F and G) The expression of anti-apoptotic Bcl-2 family proteins as indicated was detected by western blots. β-actin was detected as the loading control.

Results in (D–G) are representative of at least three independent experiments.

Tumor-specific overexpression of Bcl-xL is associated with a poor prognosis in ENKTL patients

Next, we further assessed Bcl-xL protein levels in tumor tissues from 91 cases of ENKTL patients by immunohistochemical (IHC) staining with a commercial anti-Bcl-xL antibody that specifically responded to Bcl-xL in tumor tissues compared with tumor-adjacent tissues (Figure 2A, detailed patients' information also see Table S2). The tumor regions were spatially and histologically classified by hematoxylin and eosin (H&E) staining. It is worth noting that Epstein-Barr encoded RNA (EBER) *in situ* hybridization assay is included as the gold standard for the detection and diagnosis of ENKTL, which has characteristically associated with EBV infection.[2] Further IHC scoring analysis of Bcl-xL expression levels in tumors and adjacent tissues showed that Bcl-xL was significantly upregulated in ENKTL patient tumors (Figure 2B). To gain further insight into the specific expression pattern of Bcl-xL, we also investigated the expression levels of other Bcl-2 family members in ENKTL patient cases by the IHC staining and quantitative real-time PCR. The results further supported that Bcl-xL, but not other Bcl-2 family members, was specifically upregulated in ENKTL patients at both protein level (Figure 2C) and mRNA level (Figure 2D). To assess the clinical relevance of Bcl-xL expression, we further analyzed the correlation of Bcl-xL expression with the OS in our cohort of ENKTL patients. The optimal cutoff point for the definition of Bcl-xL high/low-expression subgroups was determined based on the median value (H-score 180) of quantitative IHC analysis in the tumor group. Patient cases exhibiting an H-score <180 were pooled in the Bcl-xL low-expression group, whereas patients with a higher H-score ($\geq$ 180) were designated Bcl-xL high-expression group. The survival analysis revealed that the OS of the patients with higher expression of Bcl-xL was significantly poorer than that of the patients with lower Bcl-xL expression ($p < 0.05$; Figure 2E).

ENKTL cell highly depends on Bcl-xL for survival

To further verify the sensitivity of ENKTL cells to Bcl-xL-specific BH3-mimetic drugs, the Bcl-2 selective inhibitor ABT-199 and the Mcl-1-selective inhibitor S63845[24] were also included as controls. Our results in Figure 3A showed that A-133, A-115, and ABT-263 exhibited significant anti-proliferative activities in SNK-6 (left panel) and LY cells (right panel). A-133 and A-115 demonstrated better cellular activity than ABT-263, indicating that the cellular potency of these Bcl-xL inhibitors is likely to be positively correlated with their binding affinity to Bcl-xL.[16] Among them, A-133 exerted the most potent activity. However, high concentrations of ABT-199 and S63845 had no apparent inhibitory activity on SNK-6 and LY cells (Figure 3A). This pattern was consistent in SNK-1 and SNT-8 cells (Figure S3A). Moreover, A-133 maintained selective cell killing against ENKTL cell lines compared to normal PBMC and a panel of other cell lines derived from hematological malignancies, including leukemia and lymphoma (Figure 3B), which was consistent with the specific overexpression of Bcl-xL in ENKTL cell lines. In contrast, ABT-199 showed insensitivity to ENKTL cell lines (Figure S3B) but exhibited expected activity in known Bcl-2-dependent leukemic cell lines (i.e., HL-60, RS4; 11 cells). The detailed list of IC_{50} values (half-maximal growth inhibitory concentration) is included in Table S3. The apoptosis-inducing activity of Bcl-xL-specific BH3-mimetic drugs on SNK-6 cells was further validated utilizing Annexin V/propidium iodide (PI) staining (Figures 3C and 3D) and detection of the hallmark, including proteolytic cleavage of PARP and caspase-3 activation (Figure 3E). Consistently, A-133 and, to a lesser extent, A-115 induced more profound apoptosis than ABT-263, whereas ABT-199 and S63845 showed little activity. Likewise, a similar effect was also verified in LY cells (Figure S3C). In accordance, the specific knockdown of Bcl-xL in SNK-6 cells by two independent small interfering RNAs (siRNAs) based on the nucleofection approach induced apoptosis, and the response was further augmented following subsequent exposure to gemcitabine (Figures 3F, 3G, and S3D).

In addition, a Bcl-xL-specific proteolysis-targeting chimera (PROTAC) degrader DT2216, which has been developed as a more tolerated alternative to ABT-263 by conjugating with the von Hippel-Lindau (VHL) E3 ligase ligand,[25] was introduced into our study. We showed that DT2216 significantly induced the apoptosis of the ENKTL cells and triggered Bcl-xL protein degradation in a dose-dependent manner (Figures 3H–3J). Notably, compared with Jurkat cells, a known Bcl-xL-dependent T-cell acute lymphocytic leukemia (T-ALL) cell line, DT2216, was much less potent in degrading Bcl-xL and inducing apoptosis in SNK-6 cells, possibly due to the much lower expression level of VHL E3 ligase (Figures S3E and S3F). These results further supported that DT2216-induced Bcl-xL degradation is mediated by VHL E3 ubiquitin ligase, which is consistent with the nature of PROTAC design. Consistently, U937 cells, a Bcl-xL-independent cell line, exerted resistance to induction of apoptosis even though DT2216 achieved significant Bcl-xL degradation. Taken together, our results demonstrated the addiction of ENKTL cells to Bcl-xL for survival, and the targeted inhibition of Bcl-xL could have therapeutic benefits for ENKTL treatment.

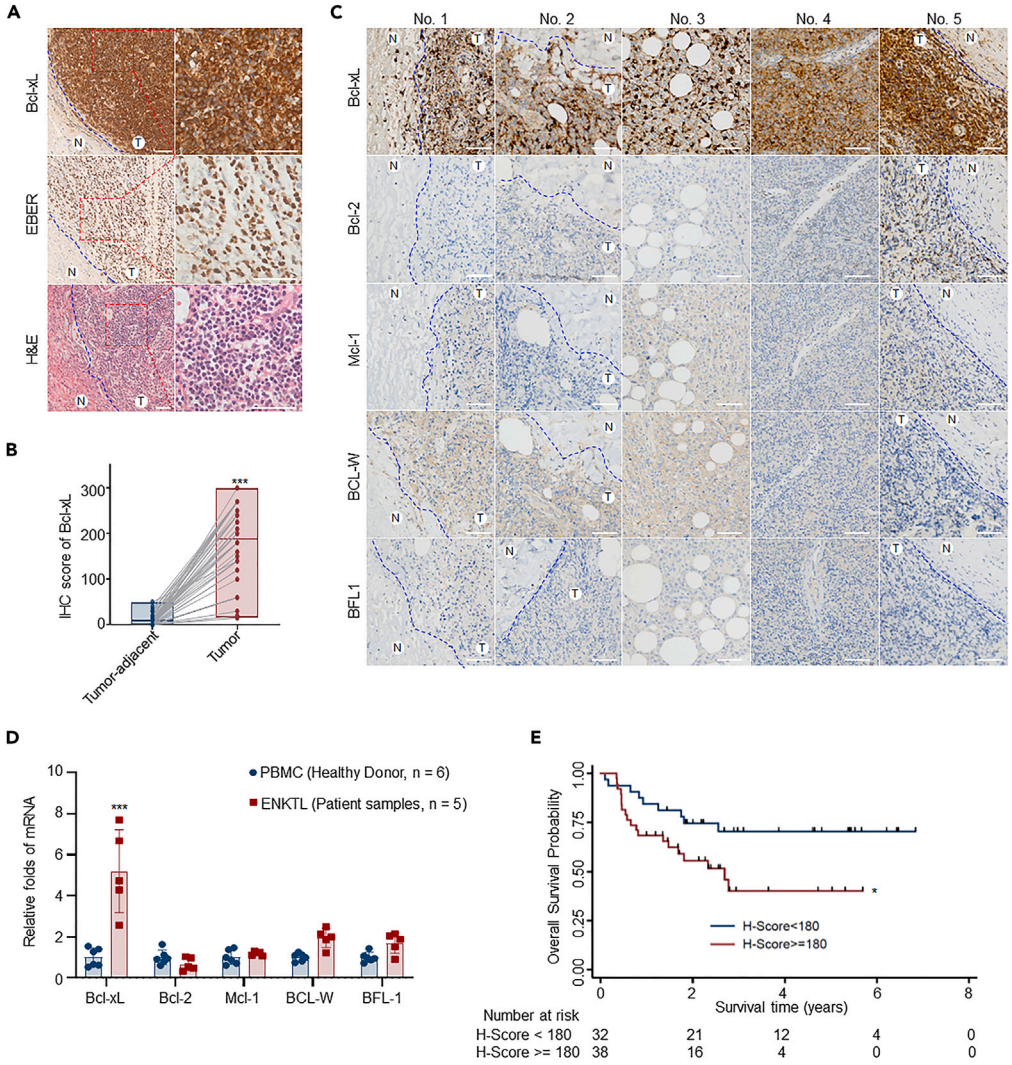

Figure 2. Specific high expression of Bcl-xL is associated with a poor prognosis in ENKTL patients

(A) Morphological and histopathological comparison of primary ENKTL biopsies. Representative images of Bcl-xL immunostaining, EBER *in situ* hybridization (indicating tumor cells), and H&E staining are shown. Scale bars, 50 μm. (T), tumor; (N), tumor-adjacent tissue.

(B) Distribution of Bcl-xL H-scores across 91 patients according to tumor and tumor-adjacent (n = 51 with tumor-adjacent). $p < 0.001$ (***) was determined by a two-tailed t test.

(C and D) Histopathological examination (C) and the mRNA expression levels (D) of anti-apoptotic Bcl-2 family proteins in 5 patient cases from the present cohort were performed by immunostaining and quantitative real-time PCR, respectively. Scale bars, 50 μm. (T), tumor; (N), tumor-adjacent tissue. Error bars represent the mean ± SD in an independent experiment. $p < 0.001$ (***) against the normal PBMC group (n = 6), two-tailed t test.

(E) Excluding patients lost to follow-up, 70 patients were included in the survival analysis. Overall survival of 70 patients for whom Bcl-xL expression was determined and divided according to those with an H-score <180 (blue line) and H-score of ≥ 180 (red line). p value was determined by the log rank test. $p < 0.05$ (*) between the two compared groups.

Activation of the IL2-JAK1/3-STAT5 pathway is associated with Bcl-xL upregulation

ENKTL initiates chronic inflammatory responses in which immune-associated pro-inflammatory cytokines (including IL-2, tumor necrosis factor alpha [TNF-α], and interferon [IFN]-γ, etc.) are overexpressed, thereby promoting lymphoma-associated hemophagocytic syndrome (LAHPS) during the progression of lymphoma, and may indicate an extremely poor outcome.[1,26] Elevated serum soluble interleukin-2 receptor (sIL-2R) level was related to poor prognosis and can be used as a valuable biomarker for disease activity.[27] In our ENKTL patient cohort, we found that sIL-2R levels were elevated in the patient group with higher

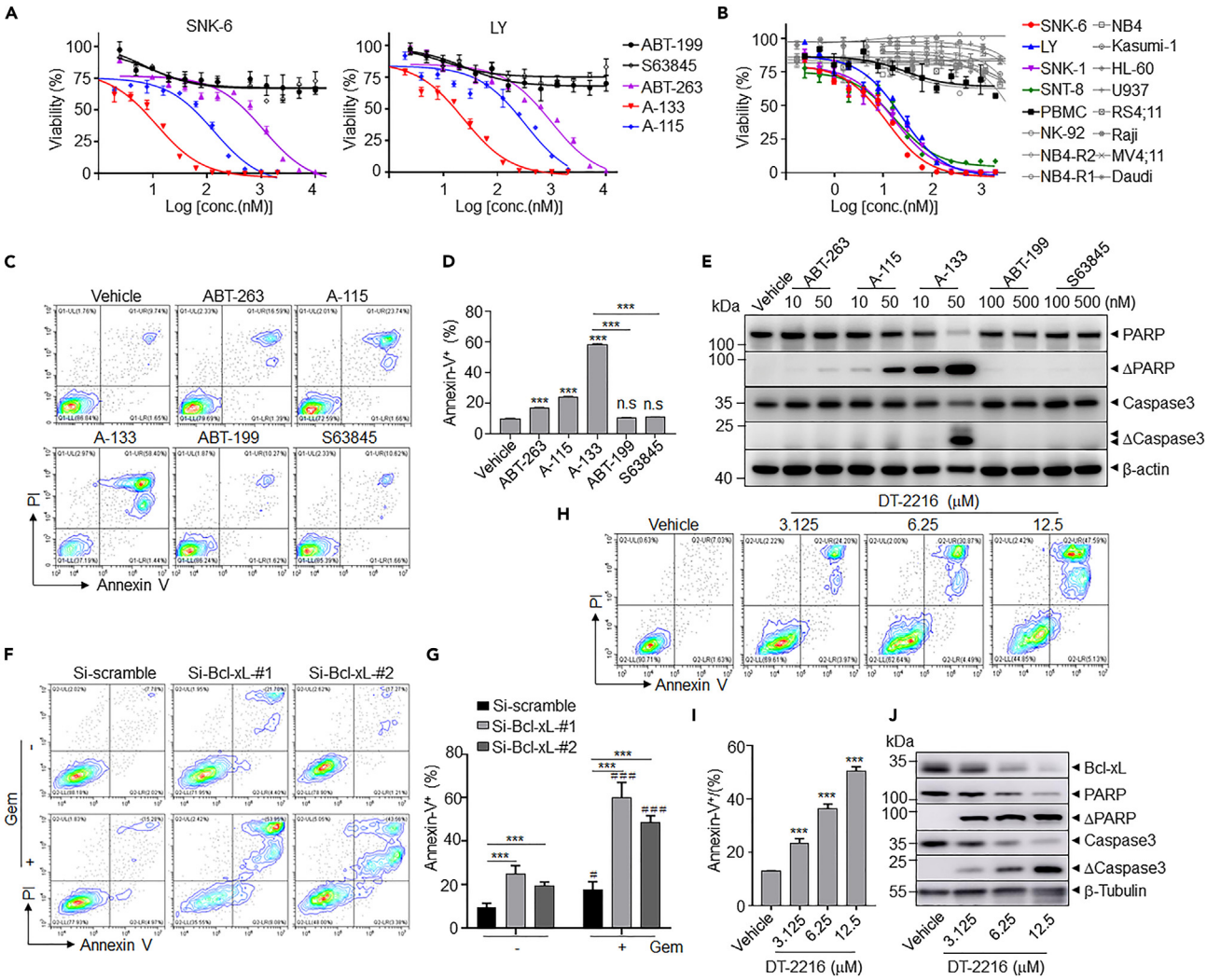

Figure 3. Inhibition of Bcl-xL preferentially induces apoptosis in ENKTL

(A) SNK-6 and LY cells were treated with different BH3-mimetic drugs, and growth inhibition was evaluated by a CCK-8 assay. ABT-263, Bcl-xL/Bcl-2 dual inhibitor; A-1331852 (A-133) and A-1155463 (A-115), Bcl-xL-specific inhibitor; ABT-199, Bcl-2-specific inhibitor; S63845, Mcl-1-specific inhibitor.

(B) Normal PBMC, ENKTL cell lines, and a panel of hematopoietic malignant cell lines were treated with A-133 at different doses, and growth inhibition was evaluated by a CCK-8 assay.

(C and D) SNK-6 cells were incubated with 50 nM of ABT-263, A-133, and A-115, as well as 500 nM of ABT-199 and S6384 for 24 h, and the apoptosis-inducing activity was evaluated by Annexin-V/PI staining (C). The percent of Annexin-V^+ cells was quantified, including the early-stage apoptotic cell population (Annexin-V^+ PI^-) and late-stage apoptotic cell population (Annexin-V^+ PI^+) (D).

(E) SNK-6 cells were incubated with different BH3-mimetic drugs at the indicated concentration, and the apoptosis-inducing activity was evaluated by western blotting.

(F and G) SNK-6 cells were nucleofected with Bcl-xL siRNA, and apoptosis was evaluated with or without 100 nM gemcitabine treatment (F). Gem, gemcitabine. The percent of Annexin-V^+ cells was quantified (G).

(H–J) SNK-6 cells were incubated with Bcl-xL-specific PROTAC (DT-2216) at the indicated concentration, and the apoptosis-inducing activity was evaluated by Annexin-V staining (H). The percent of Annexin-V^+ cells was quantified (I). The expression of proteins as indicated was detected by western blots (J). β-actin was detected as the loading control.

Error bars in (D, G, and I) represent the mean ± SD of triplicate samples in an independent experiment. Statistical significance was determined by a two-tailed t test. $p < 0.05$ (*), $p < 0.01$ (**), and $p < 0.001$ (***) against the vehicle-treated group and between the line-pointed group. $p < 0.05$ ($^{\#}$), $p < 0.01$ ($^{\#\#}$), and $p < 0.001$ ($^{\#\#\#}$) between groups in the presence or absence of gemcitabine in G. All experiments were repeated at least three times.

expression of Bcl-xL, indicating a possible correlation with IL-2 signaling (Figure 4A). Similar to normal NK cells, the majority of ENKTL cell lines require IL-2 for *in vitro* proliferation. Our data further demonstrated that withdrawal of IL-2 significantly suppressed Bcl-xL expression at both protein level (Figure 4B) and

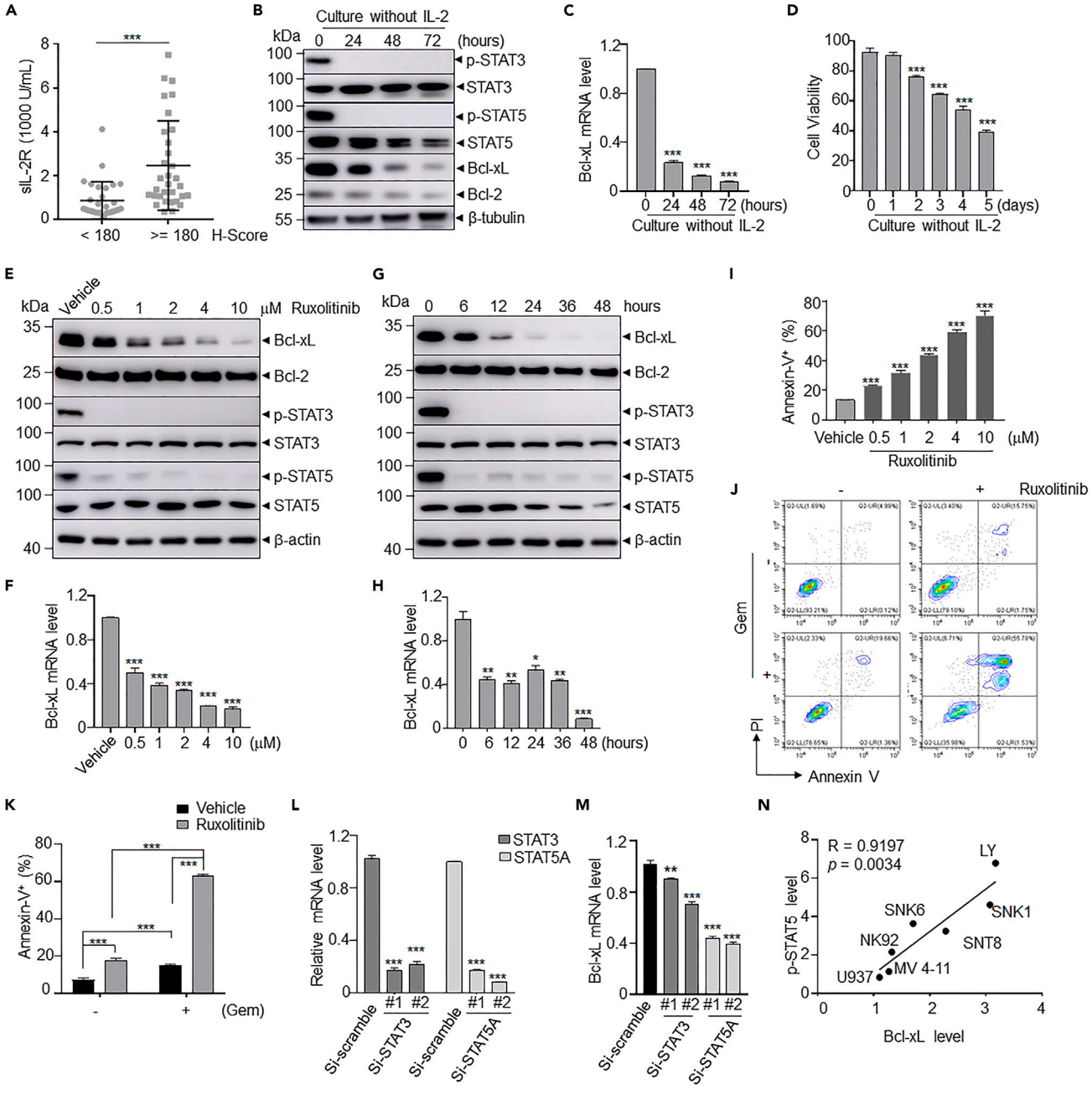

Figure 4. Upregulation of Bcl-xL involves IL2-JAK1/3-STAT5 signaling pathway in ENKTL

(A) ENKTL patient serum samples were collected and assayed for human sIL-2R concentrations by ELISA. Plots represent data from indicated cohorts of patients, n = 30 for the group with an H-score <180 and n = 32 for the group with an H-score ≥ 180. $p < 0.001$ (***) was determined by a two-tailed t test.

(B–D) SNK-6 cells were deprived of IL-2 for the indicated days, and the expression of proteins as indicated (B) and mRNA level of Bcl-xL (C) were detected by western blots and quantitative real-time PCR, respectively. The cell viability was determined by cell counting with Trypan blue (D).

(E and F) SNK-6 cells were incubated with ruxolitinib for 24 h at the indicated doses, and the expression of protein as indicated (E) and mRNA level of Bcl-xL (F) were detected by western blots and quantitative real-time PCR, respectively. β-actin was detected as the loading control.

(G and H) SNK-6 cells were incubated with ruxolitinib at 2 μM for the indicated hours, and the expression of protein as indicated (G) and mRNA level of Bcl-xL (H) were detected.

(I–K) the apoptosis-inducing activity of SNK-6 cells was evaluated with ruxolitinib treatment at the indicated concentration (I), as well as with 0.5 μM of ruxolitinib following with or without 100 nM gemcitabine treatment (J) for 48 h. Gem, gemcitabine. The percent of Annexin-V^+ cells was quantified (K).

(L and M) SNK-6 cells were nucleofected with specific siRNAs against STAT3 and STAT5A. The mRNA level of STAT3/STAT5A (L) and Bcl-xL (M) was detected by quantitative real-time PCR.

Figure 4. *Continued*

(N) The correlation between the p-STAT5 level with Bcl-xL expression was analyzed by Pearson's correlation.

Error bars in (C, D, F, H, I, and K–M) represent the mean ± SD of triplicate samples in an independent experiment. $p < 0.05$ (*), $p < 0.01$ (**), and $p < 0.001$ (***) against the vehicle-treated or si-scramble group and between the line-pointed group, two-tailed t test. Results are representative of at least three independent experiments.

mRNA level (Figure 4C) in SNK-6 cells, thus resulting in a progressive decline in cell viability (Figure 4D), further supporting the involvement of IL-2 signaling in Bcl-xL upregulation in ENKTL. Concomitantly, STAT3 and STAT5 phosphorylation (as assessed by p-STAT3 and p-STAT5) was inhibited after IL-2 deprivation (Figure 4B).

Bcl-xL regulation is tightly controlled, and several transcription factors (i.e., STATs, Rel/NF-κB, and Ets) have been demonstrated to be involved in Bcl-xL regulation.[28] On the other hand, the intracellular signal pathways activated by the IL-2, such as JAK/STAT pathway, have been well supported to be associated with ENKTL pathogenesis.[1,10] Based on the hints given above, JAK/STAT signaling inhibitor ruxolitinib (JAK1/2 inhibitor) was utilized to clarify the molecular mechanism of Bcl-xL dysregulation in ENKTL. The results showed that ruxolitinib treatment significantly decreased Bcl-xL expression at both protein and mRNA levels in SNK-6 cells in a dose-dependent (Figures 4E and 4F) and time-dependent manner (Figures 4G and 4H) in parallel with inhibition of STAT3 and STAT5 phosphorylation, indicating that the Bcl-xL expression is transcriptionally regulated by JAK-STAT signaling. Consequently, ruxolitinib treatment induced significant cell apoptosis (Figure 4I) and enhanced chemosensitivity to gemcitabine in SNK-6 cells (Figures 4J and 4K). To further investigate the participation of JAK1, JAK2, and JAK3 in Bcl-xL regulation, JAK isoform-selective inhibitors were utilized. Our data demonstrated that specific inhibitors of JAK1 (JAK1i, upadacitinib) and JAK3 (JAK3i, PF-06651600) dose-dependently (Figures S4A and S4B) and time-dependently (Figures S4D–S4F) reduced the Bcl-xL expression at both protein and mRNA levels in SNK-6 cells. However, the inhibitor of JAK2 (JAK2i, fedratinib) was much less potent in regulating Bcl-xL expression (Figure S4C). Correspondingly, JAK1i and, to a lesser extent, JAK3i exerted more potent cellular activity than JAK2i (Figure S4G). Moreover, the specific knockdown of STAT3 and STAT5 was performed to clarify their involvement. The results demonstrated that STAT5A knockdown was more potent in reducing Bcl-xL expression compared to STAT3, suggesting a more important role of STAT5 in Bcl-xL upregulation (Figures 4L and 4M). Consistently, increased baseline levels of p-STAT5 were positively correlated with higher Bcl-xL levels in ENKTL cell lines (Figures 4N and S4H). On the contrary, the levels of p-STAT3 were not significantly correlated with Bcl-xL expression (Figures S4H and S4I). Similarly, treatment of LY cells with ruxolitinib, JAK1i, and JAK3i resulted in a significant reduction of Bcl-xL at both protein and mRNA levels, whereas JAK2i was much less potent in downregulating Bcl-xL (Figures S5A–S5D). Consistently, the combination of ruxolitinib and gemcitabine significantly increased the apoptosis of LY cells (Figure S5E). Furthermore, IL-2 deprivation also suppressed Bcl-xL expression at protein and mRNA levels (Figure S5F) and a gradual increase in cell death in LY cells (Figure S5G). Collectively, all these data indicated a relevant role of the IL2-JAK1/3-STAT5 pathway in Bcl-xL dysregulation in ENKTL.

Bcl-xL inhibition significantly inhibits tumor growth and prolongs survival in the SNK-6 cell xenograft and PDX xenograft murine models

To establish a murine model of ENKTL to evaluate potential therapies of Bcl-xL inhibition *in vivo*, we transfected SNK-6 cells with the construct carrying luciferase reporter and generated SNK6-Luc cells. SNK6-Luc cells were injected intraperitoneally (i.p.) in highly immune-deficient NOD/ShiLtJGpt–Prkdc^{em26Cd52}Il2rg^{em26Cd22}/Gpt (NCG) mice, and human recombinant IL-2 was also administered to support the cell proliferation *in vivo* according to the previously reported procedure.[29] SNK6-Luc tumor-bearing NCG mice were orally administrated with A-133, ABT-263, and ABT-199 for two weeks followed by treatment cessation (Figure 5A). The dosing regimen was determined by balancing tolerability and efficacy. Dosing schedules for ABT-263, A-133, and ABT-199 were previously reported in murine xenograft models such as lung cancer and acute lymphoblastic leukemia models.[16] In our preliminary dosing testing experiment (data not shown), we observed a significant and rapid weight loss in NCG mice utilizing a previously reported dosing regimen of A-133 (25 mg/kg twice daily). Therefore, the dose of A-133 was reduced to half (25 mg/kg once daily), and a 2-week intermittent schedule for five days of consecutive administration followed by two days of rest per week (5-day-on/2-day-off) was employed to achieve tolerability and optimal anti-tumor efficacy. Similarly, ABT-263 treatment at the halved dosing of 50 mg/kg once daily showed better tolerability in NCG mice than a previously reported dosing of 100 mg/kg. Therefore, ABT-263 was administered at 50 mg/kg once daily for two weeks. ABT-199 was included as the control at the same dose as ABT-263 at 50 mg/kg once daily for two weeks, and the NCG mice were well

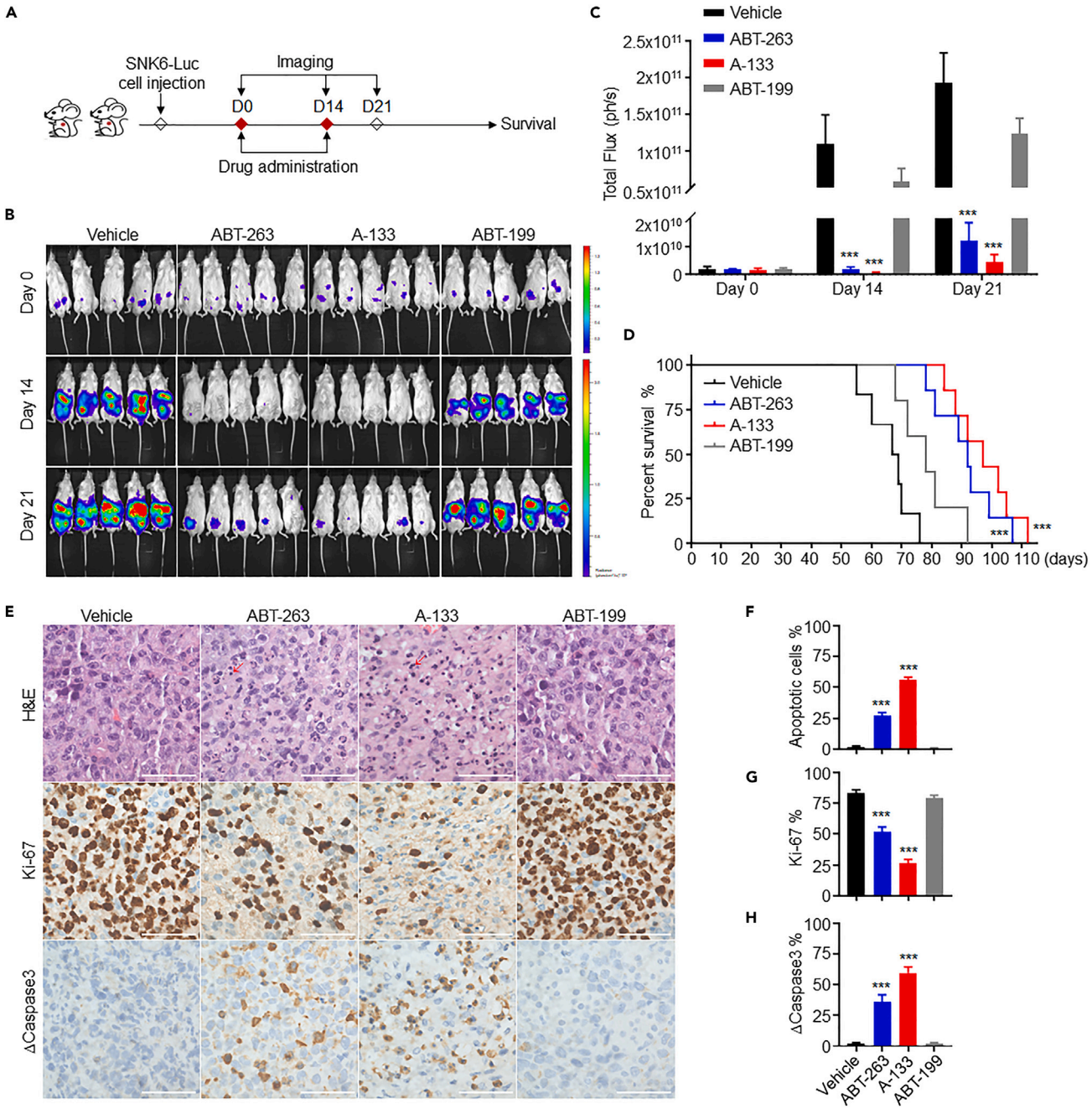

Figure 5. Inhibition of Bcl-xL demonstrates preferential activity in the CDX murine model of ENKTL

(A) Schematic of the xenograft mouse model. Luciferase-expressing SNK-6 cells were injected i.p. in NCG mice. SNK6-Luc tumor-bearing mice were grouped and treated with vehicle, ABT-263 (50 mg/kg), A-133 (25 mg/kg), and ABT-199 (50 mg/kg) for two weeks by oral administration and were observed for at least another week after drug withdrawal ($n \geq 6$ for each group). Mice were humanely euthanized at the pre-defined endpoint (see the STAR methods).

(B) SNK6-Luc tumor-bearing mice of each group were analyzed for tumor growth through bioluminescence imaging.

(C) Quantitative results were analyzed for each group and expressed as total photon values per second (Total Flux [p/s]). Error bars represent the mean ± SD in each group ($n \geq 6$ for each group). $p < 0.001$ (***) against the vehicle-treated group, two-tailed t test.

(D) The survival (%) and lifetime (days) of xenograft mice in each group were recorded ($n \geq 8$ for each group), and Kaplan-Meier survival analysis was shown. p value was determined by the log rank test. $p < 0.001$ (***) against the vehicle-treated group.

(E) Representative H&E and immunohistochemical staining of human Ki-67 and cleaved caspase-3 in tumor sections from drug-treated mice. Mice received the continuous daily treatment of different drugs at doses as indicated for four days ($n \geq 3$ for each group). All mice were humanely euthanized at 6 h after the last injection and tumor sections were harvested. Scale bars, 50 μm. The red arrow indicates apoptotic cells.

(F–H) Quantitative results were analyzed in each group for apoptotic cells (F), Ki-67 positive cells (G), and cleaved caspase-3 positive cells (H).

Error bars in (F–H) represent the mean ± SD in each group (n = 10 images per group). $p < 0.001$ (***) against the vehicle-treated group, two-tailed t test.

tolerated. ABT-263 at the dose of 50 mg/kg and A-133 at the dose of 25 mg/kg significantly delayed tumor growth by bioluminescence measurements, which were maintained even after drug discontinuation (Figures 5B and 5C). Conversely, ABT-199 at the dose of 50 mg/kg showed weak activity *in vivo*. Following drug treatment (day 14), there was a reduction in platelet numbers (Figure S6A) and body weight (Figure S6B) in either ABT-263 or A-133 treatment group due to the on-target thrombocytopenia caused by the Bcl-xL inhibition. However, the platelet counts and body weight rebounded to pre-treatment levels by the time of drug withdrawal for a week. Furthermore, therapy with ABT-263 and, to a greater extent, A-133 exerted improved therapeutic efficacy, as evidenced by the significant survival prolongation of tumor-bearing mice compared with the vehicle treatment (Figure 5D). In contrast, ABT-199-treated mice had a worse OS rate than ABT-263- and A-133-treated groups. In addition, the therapeutic efficacy of ABT-263 and A-133 *in vivo* was also supported by decreased levels of the cell proliferation marker Ki-67 and increased levels of the apoptotic markers cleaved caspase-3 in tumor sections of drug-treated mice following the continuous daily treatment for four days (Figures 5E–5H).

Utilization of PDXs as preclinical models for investigating the molecular basis of pathogenesis and identifying new therapeutics of ENKTL is urgently needed. According to the process illustrated in Figure S7A, we generated and characterized two ENKTL PDX models from two relapsed and refractory clinical patients (termed PDX-#1 and PDX-#2), corresponding to the patient cases (No. 1 and No. 2) in Figure 2C, who exhibited specific Bcl-xL high expression as demonstrated by IHC staining and quantitative real-time PCR, respectively (Figures 2C and 2D). Primary tumor tissues from the two ENKTL patients were engrafted into NCG mice, and the PDX mice showed symptoms such as a faster breathing rate, rough fur, decreased physical activity, and apparent weight loss and developed splenomegaly when the disease occurred (Figure 6A). Histological analyses showed similarities of histologic features-$CD56^{+}$ $EBER^{+}$ $Ki\text{-}67^{high}$ between PDX tumor and the parental patient biopsies (Figure 6B). Moreover, the PDX mice also displayed aggressive tumor cell tissue infiltration, with significant infiltration of human malignant tumor cells into the spleen, liver, kidney, and lung tissues accompanied by strong EBER positive signals (Figures S7B and S7C), consistent with the highly aggressive characteristic of ENKTL in the clinic. Besides the spleen, the flow cytometry analysis revealed that CD56-positive human malignant tumor cells also accumulated in the bone marrow (BM) in the PDX mice (Figure S7D). Additionally, hemophagocytosis was occasionally observed by Giemsa-Wright's staining of BM smears (Figure S7E). Besides, a comparison of the STR DNA fingerprinting analysis in tumor tissues from the two PDX models and the corresponding original patient showed very strong concordance as indicated by the percentage of identity, 97% for PDX-#1 and 100% for PDX-#2 (see Table S4). All the results above showed that the engrafted tumors from our established ENKTL PDX models faithfully represented the immunophenotypic and genetic characteristics of the original primary patient tumors. We next performed the efficacy evaluations of Bcl-xL inhibition in the two PDX models *in vivo*.

In the vehicle-treated group, the PDX-#1 mice developed the disease evidenced by splenomegaly and kidney color alteration from pink to white, suggesting a massive malignant infiltration. Targeted inhibition of Bcl-xL with ABT-263 and A-133, but not inhibition of Bcl-2 with ABT-199, significantly alleviated tumor progression and exerted therapeutic benefits in the PDX model as evidenced by morphological observation of spleen and kidney (Figure 6C). In accordance with this result, treatment of both ABT-263 and A-133 substantially inhibited the percentage of human $HLA\text{-}DR^{+}$ $CD56^{+}$ tumor cells accumulated in the spleen, BM, and kidney in opposition to the vehicle and ABT-199 treatment by flow cytometry (Figure 6D). Moreover, both A-133 and ABT-263 treatment significantly improved the survival of PDX-#1 mice *in vivo*, and A-133 showed the best survival outcomes (Figure 6E). However, ABT-199 failed to prolong the survival of PDX-#1 mice. We also investigated drug efficacy in characterized PDX-# 2 mice (Figure S7F). In the vehicle-treated group, mice showed significant infiltration of human malignant cells into the BM by flow cytometry analysis, and targeted inhibition of Bcl-xL with ABT-263 and A-133 significantly reduced tumor cell infiltration in the BM by flow cytometry (Figure 6F). Collectively, the above data indicated that targeted inhibition of Bcl-xL exhibits therapeutic promise in preclinical *in vivo* models.

Bcl-xL blockade exerts synergistic effects combined with clinical chemotherapy drugs

Due to the relative resistance of ENKTL to conventional chemotherapy, we further explored the efficacy of Bcl-xL inhibition in combination with multiple chemotherapeutic agents, including L-asparaginase (L-ASP), gemcitabine (Gem), oxaliplatin (Oxa), and etoposide (Eto), which are incorporated into multiple non-anthracycline-based ENKTL regimens. ENKTL cells were incubated with increasing concentrations of Bcl-xL inhibitors and different clinical chemotherapy drugs alone or in combination at a constant ratio for 48

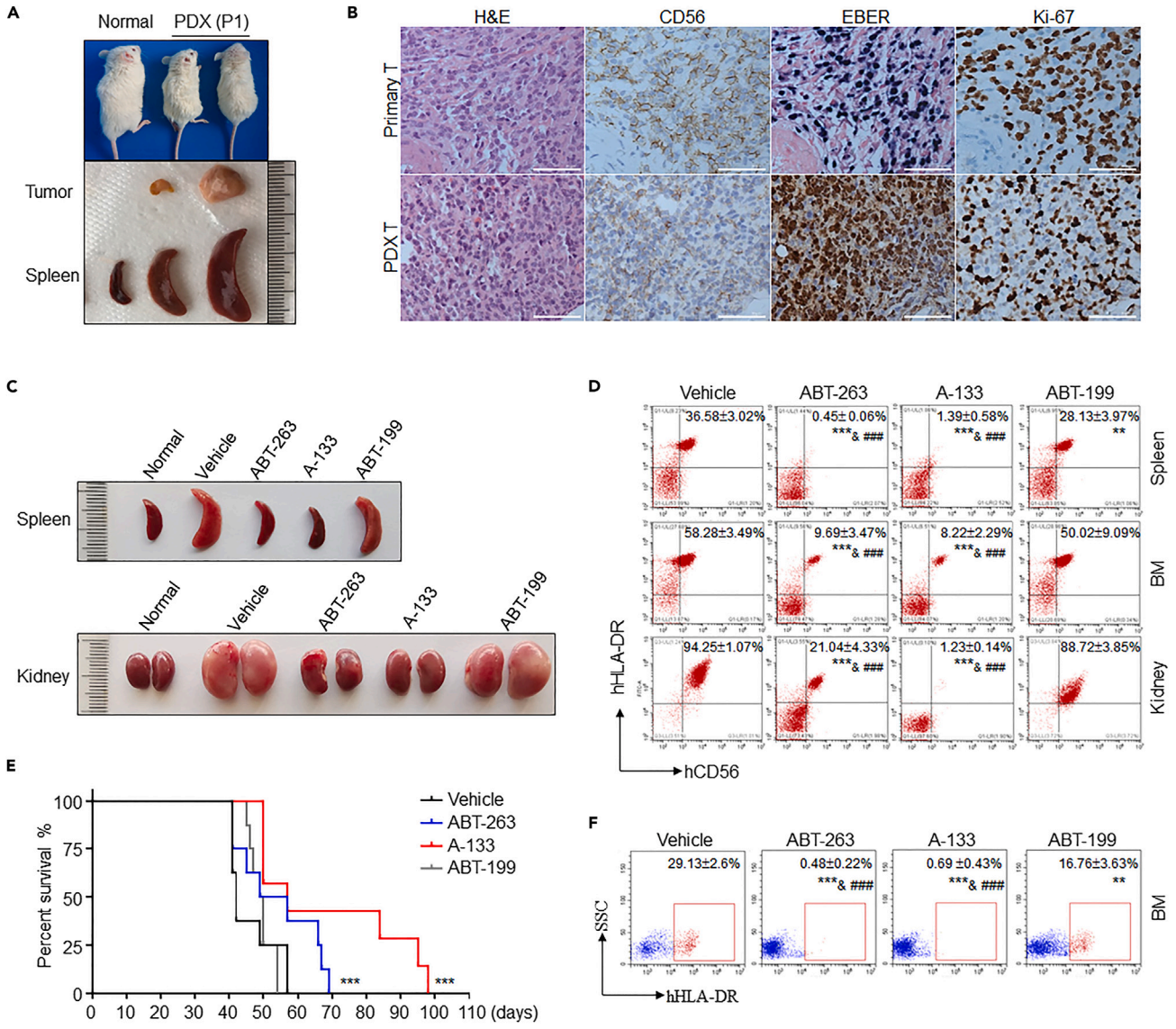

Figure 6. Inhibition of Bcl-xL exhibits potential therapeutic efficacy in PDX murine models of ENKTL

(A) The primary PDX mice were humanely euthanized at the pre-defined endpoint (see the STAR methods). The representative macroscopic appearance of normal mice and PDX-#1 (P1) mice (top), tumor, and spleens (bottom).

(B) Pathological features of the primary tumor from the patient (primary T, top) and tumor section from the PDX-#1 (P1) mice (PDX T, bottom) were characterized by H&E, CD56, EBER, and Ki-67 staining. Scale bars are 50 μm.

(C) The single-cell suspensions of spleens of P1 passage mice (PDX-#1) were transplanted to secondary recipient mice (P2 passage). These mice were treated with ABT-263 (50 mg/kg), A-133 (25 mg/kg), and ABT-199 (50 mg/kg) for two weeks by oral administration as described in Figure 5 ($n \geq 6$ for each group). The representative macroscopic appearance of the spleen (top) and kidney (bottom) in each group of PDX-#1 mice are shown.

(D) The percent of anti-human HLA-DR$^+$CD56$^+$ cells of the spleen, bone marrow (BM), and kidney cells derived from different drugs-treated PDX-#1 mice (P2 passage, $n \geq 3$ for each group) by flow cytometry.

(E) The survival (%) and lifetime (days) of different drug-treated PDX-#1 mice (P2 passage) were recorded ($n = 10$ for each group), and Kaplan-Meier survival analysis was shown. p value was determined by the log rank test. $p < 0.001$ (***) against the vehicle-treated group.

(F) The percent of anti-human HLA-DR$^+$ cells of BM cells derived from different drugs-treated PDX mice of PDX-#2 model (P2 passage, $n \geq 3$ for each group) by flow cytometry.

Data in (D and F) represent the mean ± SD in each group. Statistical significance was determined by a two-tailed t test. $p < 0.05$ (*), $p < 0.01$ (**), and $p < 0.001$ (***) against the vehicle-treated group; $p < 0.05$ (#), $p < 0.01$ (##), and $p < 0.001$ (###) against ABT-199-treated group in D and F.

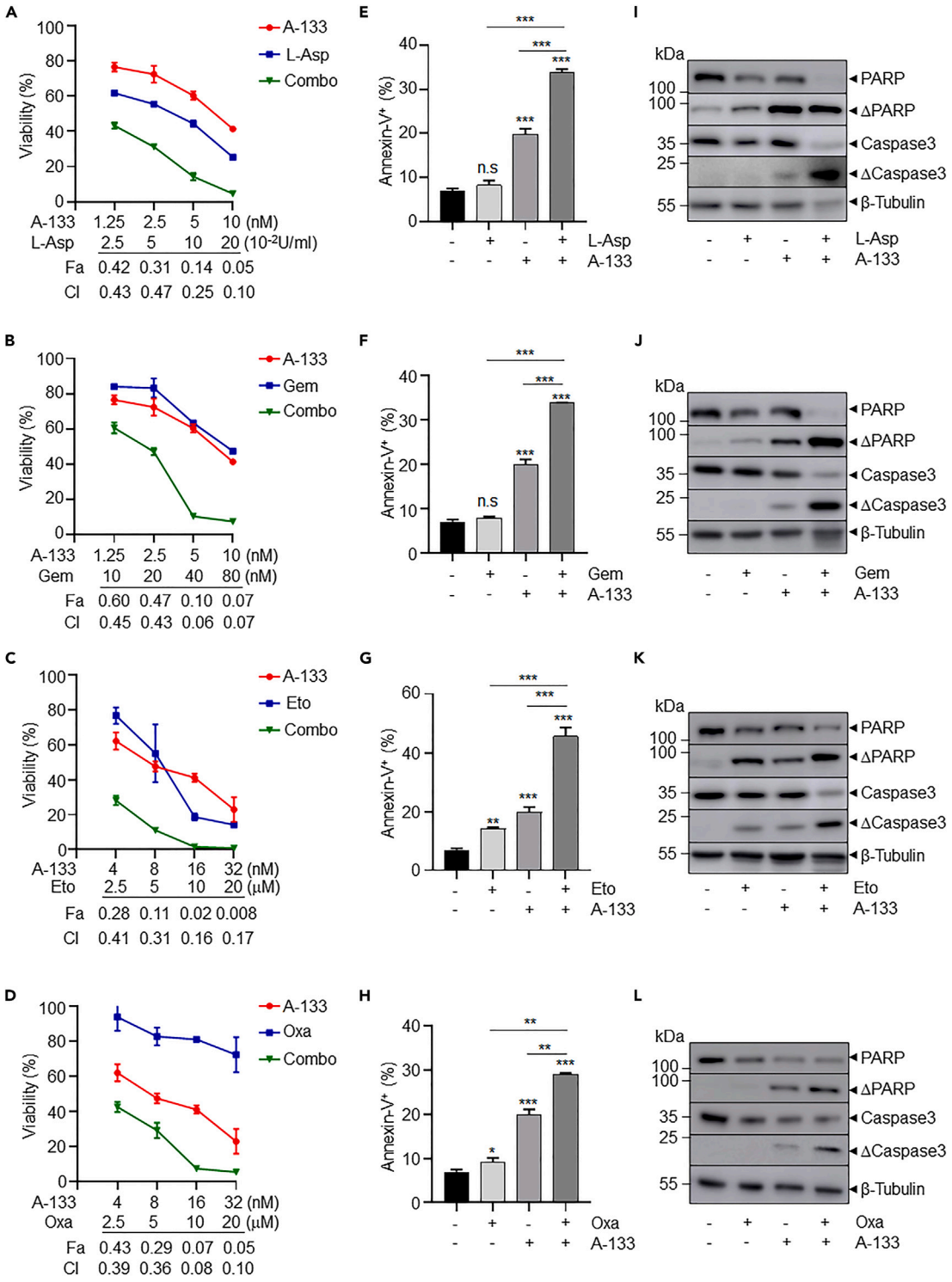

Figure 7. Bcl-xL inhibition exerts synergistic effects with clinical chemotherapy drugs

(A–D) SNK-6 cells were incubated with increasing concentrations of Bcl-xL inhibitor A-133 and different clinical chemotherapy drugs- L-Asp (A), Gem (B), Eto (C), and Oxa (D) alone or in combination for 48 h. Cell viability was determined by CCK8 assay. The CI and Fa values for the combination were calculated using the CalcuSyn software.

Figure 7. *Continued*

(E–L) SNK-6 cells were incubated with A-133 (10 nM) in the presence or absence of L-Asp (0.2 U/mL) (E & I), Gem (80 nM) (F & J), and Eto (6.25 μM) (G & K) for 24 h, as well as Oxa (6.25 μM) (H & L) for 48 h. The apoptosis-inducing activity was evaluated by Annexin-V staining (E–H) and western blotting (I–L). Error bars in (E–H) represent the mean ± SD of triplicate samples in an independent experiment. Statistical significance was determined by a two-tailed t test. $p < 0.05$ (*), $p < 0.01$ (**), and $p < 0.001$ (***) against the vehicle group and between the line-pointed group; n.s, not significant. All experiments were repeated at least three times.

h. The combination index (CI) values and fraction (Fa) values for the combination were calculated using CalcuSyn software. Compared with single drug treatment alone, the combination exhibited enhanced cytotoxicity. Our data showed that Bcl-xL blockade through A-133 exerted synergistic effects combined with these chemo-drugs with the CI value <1 in SNK-6 cells (Figures 7A–7D) and LY cells (Figures S8A–S8D). Consistently, A-133 combined with these chemotherapy agents resulted in significantly increased apoptosis in SNK-6 cells assessed by Annexin V/PI staining (Figures 7E–7H) and western blot analysis (Figures 7I–7L). Meanwhile, the combination of ABT-263 paired with these chemotherapy agents was also defined with synergistic effects on SNK-6 cells (Figures S8E–S8H) and LY cells (Figures S8I–S8L). Collectively, the data above showed that Bcl-xL inhibition sensitized ENKTL cells to chemotherapy drugs, further supporting that Bcl-xL overexpression at least partially contributes to chemotherapy resistance and that Bcl-xL inhibition could provide a potential therapeutic benefit for ENKTL treatment.

DISCUSSION

ENKTL is a unique clinicopathological entity typically associated with poor survival outcomes. However, to date, standard treatment strategies have not been defined. L-asparaginase-containing chemotherapy regimens have improved clinical outcomes in ENKTL treatment.[30] Patients who failed asparaginase-based therapy have limited treatment options with a median survival of <6 months[31] Nowadays, immune checkpoint inhibitors (anti-PD-L1/PD-1 antibodies) and targeted therapies (Histone deacetylase [HDAC] inhibitors, chidamide) have also shown promising results in early trials.[32–34] So, there is great need to identify new therapeutic targets, prognostic factors, and novel effective therapeutic agents. Here we performed high-throughput chemogenomic screening using a targeted chemical library of small molecules with known drug targets to identify potential therapeutic targets and druggable mechanisms of ENKTL.

On the one hand, our screening results revealed that inhibitors targeting HSP90, HDAC, JAK, proteasome, and PI3K, exerted good cellular potency in ENKTL cells, and these signaling pathways are well supported to be involved in ENKTL pathogenesis.[1,35] On the other hand, our screening data identified the aberrant apoptotic pathway in ENKTL pathogenesis and indicated Bcl-xL as a critical survival factor. Recently Sejic et al. have reported that the blockade of Bcl-xL induces cell apoptosis of EBV^+ T/NK cell lines.[36] However, there are several points to note. First, the cell lines utilized by Sejic et al. were derived from three different disease types of EBV-positive T/NK cell lymphoproliferative diseases (EBV-TNKLPD). EBV-TNKLPD is a group of disorders ranging from reactive lymphoproliferative diseases to fulminant malignancies. In detail, SNK-15 and SNT-16 cells were derived from chronic active EBV infection (CAEBV), a non-malignant T/NK cell proliferative disease. SNK-6 and SNT-8 cells corresponded to ENKTL, as we mentioned earlier, an EBV-related aggressive malignancy, most of NK origin and minor portion of T cell lineage. MEC04 is actually an NK leukemia cell line obtained from peripheral blood mononuclear cells of a patient who should have been diagnosed with aggressive NK cell leukemia rather than ENKTL because of the presence of 17% abnormal NK leukemia cells in the circulating blood.[37] Although they shared a common feature, the type II latency of EBV infection, previous studies have reported that additional abnormalities are likely to be involved in the malignant transformation of NK/T cells besides EBV infection.[38] The variability of Bcl-xL expression across different EBV^+ T/NK cell lines shown by Sejic et al. suggests that the pathological mechanisms of these corresponding disease types are different. In addition, we also noted some discrepancies and inconsistencies in the results reported by Sejic et al.: 1) Sejic et al. showed that Bcl-xL expression was much higher in SNK-6 and SNT-8 cells than that of CAEBV-derived SNK-15 and SNT-16 cells as well as NK-cell leukemia cell line MECO4. However, these two ENKTL cell lines were much less sensitive to Bcl-xL inhibitors than the other three cell lines, to both A-133 and ABT-737,[39] the predecessor of ABT-263. The inconsistency between Bcl-xL expression and cellular potency to Bcl-xL inhibitors does not appear to support the dependence of ENKTL on Bcl-xL. 2) Although A-133 increased tumor latency in SNK-6-tumor-bearing mice, it was ineffective in attenuating tumor burden *in vivo*. It seems difficult to explain this discrepancy regarding the limited availability of IL-2 in mice as there was no difference in the responsiveness of SNK-6 cells to A133 in the presence and absence of IL-2 *in vitro*. Therefore, it is of importance to clearly elucidate the dysregulation of Bcl-xL in ENKTL cell lines and clinical samples, the clinical significance, the functional implications *in vitro*

and *in vivo*, especially in the *in vivo* PDX models, as well as the underlying mechanism of Bcl-xL dysregulation in ENKTL.

First, we demonstrated the specific accumulation of Bcl-xL, but not other Bcl-2 family members, in ENKTL cell lines and clinical biopsies, which confers the potent efficacy of ENKTL cells to selective Bcl-xL BH3-mimetic drugs. Accordingly, Bcl-xL inhibition with A-133, A-115, and ABT-263 exhibits significant antiproliferative activity in four utilized ENKTL cell lines, including SNK-1, SNK-6, SNT-8 cells, and a new cell line LY cell, derived from our established PDX murine model. However, high concentrations of Bcl-2-specific inhibitor ABT-199 and Mcl-1-specific inhibitor S63845 had no obvious inhibitory activity on these ENKTL cells. In addition, we also show that A-133 maintained selective cell killing of ENKTL cell lines compared to normal PBMCs and a panel of other hematological malignancy cell lines. More importantly, our study uncovered the aberrant expression of Bcl-xL in ENKTL patient specimens with low survival rates and poor prognosis for the first time, supporting that Bcl-xL is a potential target for ENKTL and its inhibitors may have promising therapeutic effects. Next, we further deciphered the molecular mechanisms underlying the Bcl-xL dysregulation associated with the IL2-JAK1/3-STAT5 signaling axis. Consequently, our results further highlight the importance of JAK-STAT signaling in ENKTL, consistent with the published literature,[1,12] supporting the JAK signaling pathway as a potential therapeutic target for ENKTL. Increasing evidence has shown that the aberrant activation of the JAK-STAT pathway may be due to the overexpression or gain-of-function mutations in different components of the pathway and the stimulation of soluble growth factors or cytokines in their microenvironment, which are likely to be associated with cancer development and progression.[40] Activating mutations involving the JAK-STAT signaling pathway (mainly JAK3, STAT3, and STAT5B) have been reported in the ENKTL mutation profile and may play an important role in disease pathogenesis.[41,42] Furthermore, reports demonstrated that ruxolitinib-containing treatment could increase the clinical response rate of patients with ENKTL,[43] supporting the JAK signaling pathway as a potential therapeutic target for ENKTL. We also noticed that the apoptosis-inducing efficiency of JAKi (i.e., ruxolitinib) through downregulation of Bcl-xL expression was less potent than specific BH3 mimetics by direct inhibition of Bcl-xL activity. We speculated that since Bcl-xL is highly expressed in ENKTL cell lines, although JAKi treatment can significantly downregulate Bcl-xL, the residual Bcl-xL protein still exerts anti-apoptotic function due to the dependence of ENKTL cells on its function. This suggests that a combination of reducing Bcl-xL expression levels and inhibiting Bcl-xL activity may augment therapeutic efficacy. However, it is worth noting that inhibition of JAK signaling is accompanied by undesired systemic side effects, likely due to impaired immune cell development and function associated with JAK inhibition, such as T cells, NK cells, B cells, and dendritic cells.[44] Therefore, it is imperative to balance the positive and negative effects of JAKi therapy and define a beneficial therapeutic window. In addition, JAKi resistance often occurs, mainly due to acquired mutations in the kinase domain.[45] Thus, targeting the functionally crucial target proteins suggests new approaches to JAKi in cancer therapy. As a key downstream cell survival factor, targeting Bcl-xL might overcome resistance or intolerance to JAKi therapy. Then, we further investigated the functional role of Bcl-xL in ENKTL in preclinical studies and uncovered the addiction of ENKTL to Bcl-xL for survival *in vitro* and *in vivo*. We utilized siRNA knockdown, Bcl-xL-specific BH3 mimetics, and Bcl-xL-specific PROTAC to elucidate Bcl-xL as a key survival factor in ENKTL. Moreover, Bcl-xL inhibition sensitizes ENKTL cells to a range of chemotherapeutic agents, suggesting that Bcl-xL-mediated apoptotic resistance at least partially accounts for the chemoresistance of ENKTL. It should be noted that despite advances in cell transfection approaches, NK cells and NK cell lines remain relatively resistant to transfection, including nucleofection. In addition, Bcl-xL is predominantly highly expressed in ENKTL cell lines, and it is, therefore, challenging to achieve efficient and sufficient Bcl-xL knockdown by genetic approach in ENKTL cell lines. Partial loss of Bcl-xL expression upon siRNA knockdown compromised the induction of apoptosis but increased sensitivity to gemcitabine-induced cell apoptosis. PROTACs targeting Bcl-xL have been developed as a safe strategy to achieve robust degradation and inhibition of Bcl-xL while reducing on-target platelet toxicity due to minimal expression levels of VHL and Cereblon (CRBN) E3 ligase in platelets.[46] However, VHL-recruiting PROTAC-DT2216 exerts moderate potency to trigger Bcl-xL protein degradation and induce apoptosis in ENKTL cells, possibly due to the low expression level of VHL E3 ligase. Therefore, future attempts can be made to evaluate the expression of CRBN in ENKTL cells and the activity of CRBN-based PROTAC targeting Bcl-xL, such as XZ424 and XZ739[46] *in vitro* and *in vivo*.

Furthermore, we carefully managed the utilization of Bcl-xL inhibitors in our *in vivo* studies and demonstrated the excellent efficacy of Bcl-xL inhibition on the CDX and PDX murine models *in vivo*.

The doses of ABT-263 and A-133 were half of those previously reported in lung cancer and acute lymphoblastic leukemia models,[16] suggesting a better safety profile. Although decreased platelet counts due to Bcl-xL inhibition were also observed, platelet counts and body weight rebounded to pre-treatment levels once the drug was discontinued. A clinical study demonstrated the promising efficacy of ABT-263 in a phase 1 dose-escalation study in lymphoid malignancies (ClinicalTrials.gov, NCT00406809). In the study, 10 of 46 patients with evaluable disease had partial responses, including one patient with ENKTL and 9 patients with chronic lymphoid leukemia (CLL)/small lymphocytic lymphoma (SLL) or follicular lymphoma (FL).[47] The clinical benefit in CLL/SLL and FL patients was mainly associated with Bcl-2 inhibition by ABT-263. Based on our findings, we speculate that the ENKTL patient may benefit from ABT-263-mediated Bcl-xL inhibition. However, ABT-263 failed in clinical trials due to its on-target platelet toxicity, likely due to the essential role of Bcl-xL protein in the survival of human platelets.[48,49] Therefore, the application of other tolerated alternative strategies to reduce the on-target platelet toxicity of Bcl-xL inhibitors can also be considered[50]: i.e., highly potent Bcl-xL degrader (PROTAC), Bcl-xL-targeting antibody-drug conjugate (ADC), prodrug-based approaches (APG-1252), and Bcl-xL inhibitor-based combination therapies. A phosphate prodrug (APG-1252) was developed as a dual Bcl-xL/Bcl-2 inhibitor that was less cell permeable to platelets than cancer cells. Upon reaching cancer cells, APG-1252 is converted to APG -1252-M1, an active form, to induce cancer cell apoptosis. Compared with ABT-263, APG-1252 has more potent anti-tumor activity but less thrombocytopenic toxicity and is currently in clinical trials in various solid tumors. Based on these findings, we will explore an open-label, multi-center phase Ib/II study of the safety, pharmacokinetic (PK), pharmacodynamic (PD), and efficacy of APG-1252, a novel targeted Bcl-xL/Bcl-2 inhibitor developed by Ascentage Pharma, as a single agent or in combination with chidamide in relapsed/refractory peripheral T cell lymphomas (PTCLs) patients, including ENKTL. This study was registered at www.clinicaltrials.gov as NCT05186012.

Limitations of the study

The number of *in vitro* cell lines and CDX models utilized in this study is limited, due to the restricted availability of cell lines for ENKTL, a rare disease type. Future research will necessitate the expansion of ENKTL cell lines, particularly those with xenograft potential *in vivo*.

Given the targeted platelet toxicity of Bcl-xL inhibitors, the development of alternative strategies to reduce toxicity and enhance clinical treatment benefits is a promising approach. Although our study demonstrates the biological activity of specific PROTACs targeting Bcl-xL and the synergistic effects of Bcl-xL inhibition combined with clinical chemotherapeutic drugs at the cellular level, the translation of *in vitro* activity to *in vivo* efficacy warrants further investigation. Evaluating treatment regimens to determine the optimal balance between tolerability and effectiveness is essential.

Our research sheds light on the upstream regulatory mechanisms of Bcl-xL dysregulation; however, the *in vivo* anti-tumor activity resulting from targeting the underlying mechanism remains to be explored. The potential therapeutic benefits of targeting the upstream regulatory mechanism *in vivo* and the feasibility of combinatorial treatment approaches involving both the reduction of Bcl-xL expression levels and the inhibition of Bcl-xL activity call for further investigation in future studies.

STAR★METHODS

Detailed methods are provided in the online version of this paper and include the following:

- KEY RESOURCES TABLE
- RESOURCE AVAILABILITY
  - Lead contact
  - Materials availability
  - Data and code availability
- EXPERIMENTAL MODEL AND STUDY PARTICIPANT DETAILS
  - Cell lines and cell culture
  - Animals
  - Human subjects
- METHOD DETAILS
  - Primary cell isolation

- High throughput compound screening
- Cell growth inhibition
- Cell apoptosis
- Immunohistochemistry
- Western blotting
- Quantitative real-time PCR
- RNA interference
- Short tandem repeat (STR) analysis
- Establishment and analysis of CDX xenograft model
- Establishment and analysis of PDX xenograft models
- Establishment and characterization of LY cells
- Synergy calculations

- QUANTIFICATION AND STATISTICAL ANALYSIS
- ADDITIONAL RESOURCES

SUPPLEMENTAL INFORMATION

Supplemental information can be found online at https://doi.org/10.1016/j.isci.2023.107369.

ACKNOWLEDGMENTS

We sincerely appreciate prof. Norio Shimizu at Tokyo Medical and Dental University for providing us with SNK-1, SNK-6, and SNT-8 cells. We are also grateful to the Discovery Technology Platform and Analytical platform of Shanghai Institute for Advanced Immunochemical Studies of ShanghaiTech University for technical assistance with compound screening and flow cytometry experiments; the Molecular Imaging Core Facility platform for the School of Life Science and Technology of ShanghaiTech University for technical assistance with imaging experiment; and the staff members of the National Facility for Protein Science in Shanghai (NFPS) of Zhangjiang Lab for providing technical support and assistance in animal handling, data collection, and analysis. This research was also supported by Shanghai Frontiers Science Center for Biomacromolecules and Precision Medicine at ShanghaiTech University. This work was partially supported by grants from the National Natural Science Foundation of China (82270196 to R.T.; 81873436 to C.-X.L.; 81702600 to Q.-Q.Y.), the Outstanding Young Medical Talents Program of Shanghai Municipal Health Commission (2017YQ061 to C.-X.L.), Shanghai Sailing Program (17YF1412200 to Q.-Q.Y.), the Shanghai Municipal Education Commission-Gaofeng Clinical Medicine Grant (20152219 to R.T.), the Shanghai Science and Technology Commission Grant (18411968300 to R.T.; 23141902900 to C.-X.L.), and the Shanghai Hospital Development Center Grant (SHDC2019X02 to R.T.).

AUTHOR CONTRIBUTIONS

Conceptualization, C.X.L., G.Y.L., Q.Q.Y., and R.T.; Methodology, C.X.L., X.Y.D., G.Y.L., Z.L.X., Y.Q.Z., Y.T.C., Y.P.Z., Y.B.S., and L.Y.L.; Formal analysis, C.X.L., X.Y.D., G.Y.L., Y.T.C., Y.Q.Z., W.B.G., and Q.Q.Y.; Investigation, C.X.L., X.Y.D., G.Y.L., Y.T.C., W.B.G., and Q.Q.Y.; Resources, W.H.Z., Y.J.M., W.B.G., L.F.W., Z.L.X., and B.J.; Writing-Original Draft, C.X.L. and Q.Q.Y.; Writing-Review & Editing, C.X.L., Q.Q.Y., and R.T.; Funding Acquisition, C.X.L., B.J., Q.Q.Y., and R.T.; Supervision, B.J., Q.Q.Y., and R.T.

DECLARATION OF INTERESTS

The authors declare no competing interests.

INCLUSION AND DIVERSITY

We support inclusive, diverse, and equitable conduct of research.

Received: May 1, 2023
Revised: June 21, 2023
Accepted: July 10, 2023
Published: July 13, 2023

REFERENCES

1. Cai, Q., Cai, J., Fang, Y., and Young, K.H. (2019). Epstein-Barr virus-positive natural killer/t-cell lymphoma. Front. Oncol. *9*, 386. https://doi.org/10.3389/fonc.2019.00386.

2. Tse, E., and Kwong, Y.L. (2017). The diagnosis and management of NK/T-cell lymphomas. J. Hematol. Oncol. *10*, 85. https://doi.org/10.1186/s13045-017-0452-9.

3. Jeong, S.H. (2020). Extranodal NK/T cell lymphoma. Blood Res. *55*, S63–S71. https://doi.org/10.5045/br.2020.S011.

4. Li, X., Cui, Y., Sun, Z., Zhang, L., Li, L., Wang, X., Wu, J., Fu, X., Ma, W., Zhang, X., et al. (2016). DDGP versus SMILE in newly diagnosed advanced natural killer/t-cell lymphoma: a randomized controlled, multicenter, open-label study in China. Clin. Cancer Res. *22*, 5223–5228. https://doi.org/10.1158/1078-0432.CCR-16-0153.

5. Kim, S.J., Park, S., Kang, E.S., Choi, J.Y., Lim, D.H., Ko, Y.H., and Kim, W.S. (2015). Induction treatment with SMILE and consolidation with autologous stem cell transplantation for newly diagnosed stage IV extranodal natural killer/T-cell lymphoma patients. Ann. Hematol. *94*, 71–78. https://doi.org/10.1007/s00277-014-2171-4.

6. Liu, C., Ding, H., Zhu, Q., Liu, P., Zhu, Y., Wang, L., Ma, Y., Zhang, W., Tian, S., Zhang, X., et al. (2022). Induction with MEDA regimen and consolidation with Auto-HSCT for stage IV NKTCL patients: a prospective multicenter study. Int. J. Cancer *151*, 752–763. https://doi.org/10.1002/ijc.34055.

7. Zhu, Y., Tian, S., Xu, L., Ma, Y., Zhang, W., Wang, L., Jin, L., Liu, C., Zhu, C., Li, Z., et al. (2022). GELAD chemotherapy with sandwiched radiotherapy for patients with newly diagnosed stage IE/IIE natural killer/T-cell lymphoma: a prospective multicentre study. Br. J. Haematol. *196*, 939–946. https://doi.org/10.1111/bjh.17960.

8. Saeed, H., and Sokol, L. (2021). Extranodal NK/T cell lymphoma: evidence-based review of safety and toxicity of the available regimens. Clin. Lymphoma Myeloma Leuk. *21*, 199–204. https://doi.org/10.1016/j.clml.2020.10.006.

9. Yamaguchi, M., and Miyazaki, K. (2017). Current treatment approaches for NK/T-cell lymphoma. J. Clin. Exp. Hematop. *57*, 98–108. https://doi.org/10.3960/jslrt.17018.

10. Xiong, J., Cui, B.W., Wang, N., Dai, Y.T., Zhang, H., Wang, C.F., Zhong, H.J., Cheng, S., Ou-Yang, B.S., Hu, Y., et al. (2020). Genomic and transcriptomic characterization of natural killer t cell lymphoma. Cancer Cell *37*, 403–419.e6. https://doi.org/10.1016/j.ccell.2020.02.005.

11. Xiong, J., and Zhao, W.L. (2018). Advances in multiple omics of natural-killer/T cell lymphoma. J. Hematol. Oncol. *11*, 134. https://doi.org/10.1186/s13045-018-0678-1.

12. de Mel, S., Hue, S.S.S., Jeyasekharan, A.D., Chng, W.J., and Ng, S.B. (2019). Molecular pathogenic pathways in extranodal NK/T cell lymphoma. J. Hematol. Oncol. *12*, 33. https://doi.org/10.1186/s13045-019-0716-7.

13. Jo, J.C., Kim, M., Choi, Y., Kim, H.J., Kim, J.E., Chae, S.W., Kim, H., and Cha, H.J. (2017). Expression of programmed cell death 1 and programmed cell death ligand 1 in extranodal NK/T-cell lymphoma, nasal type. Ann. Hematol. *96*, 25–31. https://doi.org/10.1007/s00277-016-2818-4.

14. Warren, C.F.A., Wong-Brown, M.W., and Bowden, N.A. (2019). BCL-2 family isoforms in apoptosis and cancer. Cell Death Dis. *10*, 177. https://doi.org/10.1038/s41419-019-1407-6.

15. Opferman, J.T. (2016). Attacking cancer's Achilles heel: antagonism of anti-apoptotic BCL-2 family members. FEBS J. *283*, 2661–2675. https://doi.org/10.1111/febs.13472.

16. Leverson, J.D., Phillips, D.C., Mitten, M.J., Boghaert, E.R., Diaz, D., Tahir, S.K., Belmont, L.D., Nimmer, P., Xiao, Y., Ma, X.M., et al. (2015). Exploiting selective BCL-2 family inhibitors to dissect cell survival dependencies and define improved strategies for cancer therapy. Sci. Transl. Med. *7*, 279ra40. https://doi.org/10.1126/scitranslmed.aaa4642.

17. Diepstraten, S.T., Anderson, M.A., Czabotar, P.E., Lessene, G., Strasser, A., and Kelly, G.L. (2022). The manipulation of apoptosis for cancer therapy using BH3-mimetic drugs. Nat. Rev. Cancer *22*, 45–64. https://doi.org/10.1038/s41568-021-00407-4.

18. Scherr, A.L., Gdynia, G., Salou, M., Radhakrishnan, P., Duglova, K., Heller, A., Keim, S., Kautz, N., Jassowicz, A., Elssner, C., et al. (2016). Bcl-xL is an oncogenic driver in colorectal cancer. Cell Death Dis. *7*, e2342. https://doi.org/10.1038/cddis.2016.233.

19. Zhang, M., Mathews Griner, L.A., Ju, W., Duveau, D.Y., Guha, R., Petrus, M.N., Wen, B., Maeda, M., Shinn, P., Ferrer, M., et al. (2015). Selective targeting of JAK/STAT signaling is potentiated by Bcl-xL blockade in IL-2-dependent adult T-cell leukemia. Proc. Natl. Acad. Sci. USA *112*, 12480–12485. https://doi.org/10.1073/pnas.1516208112.

20. Petiti, J., Lo Iacono, M., Rosso, V., Andreani, G., Jovanovski, A., Podestà, M., Lame, D., Gobbi, M.D., Fava, C., Saglio, G., et al. (2020). Bcl-xL represents a therapeutic target in Philadelphia negative myeloproliferative neoplasms. J. Cell Mol. Med. *24*, 10978–10986. https://doi.org/10.1111/jcmm.15730.

21. Nagata, H., Konno, A., Kimura, N., Zhang, Y., Kimura, M., Demachi, A., Sekine, T., Yamamoto, K., and Shimizu, N. (2001). Characterization of novel natural killer (NK)-cell and gammadelta T-cell lines established from primary lesions of nasal T/NK-cell lymphomas associated with the Epstein-Barr virus. Blood *97*, 708–713. https://doi.org/10.1182/blood.v97.3.708.

22. Zhang, Y., Nagata, H., Ikeuchi, T., Mukai, H., Oyoshi, M.K., Demachi, A., Morio, T., Wakiguchi, H., Kimura, N., Shimizu, N., and Yamamoto, K. (2003). Common cytological and cytogenetic features of Epstein-Barr virus (EBV)-positive natural killer (NK) cells and cell lines derived from patients with nasal T/NK-cell lymphomas, chronic active EBV infection and hydroa vacciniforme-like eruptions. Br. J. Haematol. *121*, 805–814. https://doi.org/10.1046/j.1365-2141.2003.04359.x.

23. Souers, A.J., Leverson, J.D., Boghaert, E.R., Ackler, S.L., Catron, N.D., Chen, J., Dayton, B.D., Ding, H., Enschede, S.H., Fairbrother, W.J., et al. (2013). ABT-199, a potent and selective BCL-2 inhibitor, achieves antitumor activity while sparing platelets. Nat. Med. *19*, 202–208. https://doi.org/10.1038/nm.3048.

24. Letai, A. (2016). S63845, an MCL-1 selective BH3 mimetic: another arrow in our quiver. Cancer Cell *30*, 834–835. https://doi.org/10.1016/j.ccell.2016.11.016.

25. Khan, S., Zhang, X., Lv, D., Zhang, Q., He, Y., Zhang, P., Liu, X., Thummuri, D., Yuan, Y., Wiegand, J.S., et al. (2019). A selective BCL-XL PROTAC degrader achieves safe and potent antitumor activity. Nat. Med. *25*, 1938–1947. https://doi.org/10.1038/s41591-019-0668-z.

26. Huang, H., Chen, L.M., Fang, X.J., Guo, C.C., Lin, X.P., Hong, H.M., Li, X., Wang, Z., Tian, Y., Chen, M.T., et al. (2020). Prognostic value of the modified systemic in fl ammation score in patients with extranodal natural killer/T-cell lymphoma. Front. Pharmacol. *11*, 593392. https://doi.org/10.3389/fphar.2020.593392.

27. Yamaguchi, M., Suzuki, R., Oguchi, M., Asano, N., Amaki, J., Akiba, T., Maeda, T., Itasaka, S., Kubota, N., Saito, Y., et al. (2017). Treatments and outcomes of patients with extranodal natural killer/T-cell lymphoma diagnosed between 2000 and 2013: a cooperative study in Japan. J. Clin. Oncol. *35*, 32–39. https://doi.org/10.1200/JCO.2016.68.1619.

28. Morales-Martínez, M., and Vega, M.I. (2022). Roles and regulation of BCL-xL in hematological malignancies. Int. J. Mol. Sci. *23*, 2193. https://doi.org/10.3390/ijms23042193.

29. Wen, H., Ma, H., Cai, Q., Lin, S., Lei, X., He, B., Wu, S., Wang, Z., Gao, Y., Liu, W., et al. (2018). Recurrent ECSIT mutation encoding V140A triggers hyperinflammation and promotes hemophagocytic syndrome in extranodal NK/T cell lymphoma. Nat. Med. *24*, 154–164. https://doi.org/10.1038/nm.4456.

30. Fox, C.P., Civallero, M., Ko, Y.H., Manni, M., Skrypets, T., Pileri, S., Kim, S.J., Cabrera, M.E., Shustov, A.R., Chiattone, C.S., et al. (2020). Survival outcomes of patients with extranodal natural-killer T-cell lymphoma: a prospective cohort study from the international T-cell Project. Lancet. Haematol. *7*, e284–e294. https://doi.org/10.1016/S2352-3026(19)30283-2.

31. Lim, S.H., Hong, J.Y., Lim, S.T., Hong, H., Arnoud, J., Zhao, W., Yoon, D.H., Tang, T., Cho, J., Park, S., et al. (2017). Beyond first-line non-anthracycline-based chemotherapy for extranodal NK/T-cell lymphoma: clinical outcome and current perspectives on salvage therapy for patients after first relapse and progression of disease. Ann. Oncol. *28*, 2199–

2205. https://doi.org/10.1093/annonc/mdx316.

32. Tao, R., Fan, L., Song, Y., Hu, Y., Zhang, W., Wang, Y., Xu, W., and Li, J. (2021). Sintilimab for relapsed/refractory extranodal NK/T cell lymphoma: a multicenter, single-arm, phase 2 trial (ORIENT-4). Signal Transduct. Target. Ther. *6*, 365. https://doi.org/10.1038/s41392-021-00768-0.

33. Kim, S.J., Lim, J.Q., Laurensia, Y., Cho, J., Yoon, S.E., Lee, J.Y., Ryu, K.J., Ko, Y.H., Koh, Y., Cho, D., et al. (2020). Avelumab for the treatment of relapsed or refractory extranodal NK/T-cell lymphoma: an open-label phase 2 study. Blood *136*, 2754–2763. https://doi.org/10.1182/blood.2020007247.

34. Shi, Y., Dong, M., Hong, X., Zhang, W., Feng, J., Zhu, J., Yu, L., Ke, X., Huang, H., Shen, Z., et al. (2015). Results from a multicenter, open-label, pivotal phase II study of chidamide in relapsed or refractory peripheral T-cell lymphoma. Ann. Oncol. *26*, 1766–1771. https://doi.org/10.1093/annonc/mdv237.

35. Mundy-Bosse, B.L., Weigel, C., Wu, Y.Z., Abdelbaky, S., Youssef, Y., Casas, S.B., Polley, N., Ernst, G., Young, K.A., McConnell, K.K., et al. (2022). Identification and targeting of the developmental blockade in extranodal natural killer/T-cell lymphoma. Blood Cancer Discov. *3*, 154–169. https://doi.org/10.1158/2643-3230.BCD-21-0098.

36. Sejic, N., George, L.C., Tierney, R.J., Chang, C., Kondrashova, O., MacKinnon, R.N., Lan, P., Bell, A.I., Lessene, G., Long, H.M., et al. (2020). BCL-XL inhibition by BH3-mimetic drugs induces apoptosis in models of Epstein-Barr virus-associated T/NK-cell lymphoma. Blood Adv. *4*, 4775–4787. https://doi.org/10.1182/bloodadvances.2020002446.

37. Coppo, P., Gouilleux-Gruart, V., Huang, Y., Bouhlal, H., Bouamar, H., Bouchet, S., Perrot, C., Vieillard, V., Dartigues, P., Gaulard, P., et al. (2009). STAT3 transcription factor is constitutively activated and is oncogenic in nasal-type NK/T-cell lymphoma. Leukemia *23*, 1667–1678. https://doi.org/10.1038/leu.2009.91.

38. Kimura, H. (2018). EBV in T-/NK-cell tumorigenesis. Adv. Exp. Med. Biol. *1045*, 459–475. https://doi.org/10.1007/978-981-10-7230-7_21.

39. Oltersdorf, T., Elmore, S.W., Shoemaker, A.R., Armstrong, R.C., Augeri, D.J., Belli, B.A., Bruncko, M., Deckwerth, T.L., Dinges, J., Hajduk, P.J., et al. (2005). An inhibitor of Bcl-2 family proteins induces regression of solid tumours. Nature *435*, 677–681. https://doi.org/10.1038/nature03579.

40. Hu, X., Li, J., Fu, M., Zhao, X., and Wang, W. (2021). The JAK/STAT signaling pathway: from bench to clinic. Signal Transduct. Target. Ther. *6*, 402. https://doi.org/10.1038/s41392-021-00791-1.

41. Bouchekioua, A., Scourzic, L., de Wever, O., Zhang, Y., Cervera, P., Aline-Fardin, A., Mercher, T., Gaulard, P., Nyga, R., Jeziorowska, D., et al. (2014). JAK3 deregulation by activating mutations confers invasive growth advantage in extranodal nasal-type natural killer cell lymphoma. Leukemia *28*, 338–348. https://doi.org/10.1038/leu.2013.157.

42. Küçük, C., Jiang, B., Hu, X., Zhang, W., Chan, J.K.C., Xiao, W., Lack, N., Alkan, C., Williams, J.C., Avery, K.N., et al. (2015). Activating mutations of STAT5B and STAT3 in lymphomas derived from gammadelta-T or NK cells. Nat. Commun. *6*, 6025. https://doi.org/10.1038/ncomms7025.

43. Zhou, L., Liu, Y., Wen, Z., Yang, S., Li, M., Zhu, Q., Qiu, S., Gao, Y., Wang, H., Yuan, Y., et al. (2020). Ruxolitinib combined with doxorubicin, etoposide, and dexamethasone for the treatment of the lymphoma-associated hemophagocytic syndrome. J. Cancer Res. Clin. Oncol. *146*, 3063–3074. https://doi.org/10.1007/s00432-020-03301-y.

44. Groner, B., and von Manstein, V. (2017). Jak Stat signaling and cancer: opportunities, benefits and side effects of targeted inhibition. Mol. Cell. Endocrinol. *451*, 1–14. https://doi.org/10.1016/j.mce.2017.05.033.

45. Downes, C.E.J., McClure, B.J., Bruning, J.B., Page, E., Breen, J., Rehn, J., Yeung, D.T., and White, D.L. (2021). Acquired JAK2 mutations confer resistance to JAK inhibitors in cell models of acute lymphoblastic leukemia. NPJ Precis. Oncol. *5*, 75. https://doi.org/10.1038/s41698-021-00215-x.

46. Zhang, P., Zhang, X., Liu, X., Khan, S., Zhou, D., and Zheng, G. (2020). PROTACs are effective in addressing the platelet toxicity associated with BCL-XL inhibitors. Explor. Target. Antitumor. Ther. *1*, 259–272. https://doi.org/10.37349/etat.2020.00017.

47. Wilson, W.H., O'Connor, O.A., Czuczman, M.S., LaCasce, A.S., Gerecitano, J.F., Leonard, J.P., Tulpule, A., Dunleavy, K., Xiong, H., Chiu, Y.L., et al. (2010). Navitoclax, a targeted high-affinity inhibitor of BCL-2, in lymphoid malignancies: a phase 1 dose-escalation study of safety, pharmacokinetics, pharmacodynamics, and antitumour activity. Lancet Oncol. *11*, 1149–1159. https://doi.org/10.1016/S1470-2045(10)70261-8.

48. Mason, K.D., Carpinelli, M.R., Fletcher, J.I., Collinge, J.E., Hilton, A.A., Ellis, S., Kelly, P.N., Ekert, P.G., Metcalf, D., Roberts, A.W., et al. (2007). Programmed anuclear cell death delimits platelet life span. Cell *128*, 1173–1186. https://doi.org/10.1016/j.cell.2007.01.037.

49. Kaefer, A., Yang, J., Noertersheuser, P., Mensing, S., Humerickhouse, R., Awni, W., and Xiong, H. (2014). Mechanism-based pharmacokinetic/pharmacodynamic meta-analysis of navitoclax (ABT-263) induced thrombocytopenia. Cancer Chemother. Pharmacol. *74*, 593–602. https://doi.org/10.1007/s00280-014-2530-9.

50. Negi, A., and Voisin-Chiret, A.S. (2022). Strategies to reduce the on-target platelet toxicity of Bcl-xL inhibitors: PROTACs, SNIPERs and Prodrug-based approaches. Chembiochem *23*, e202100689. https://doi.org/10.1002/cbic.202100689.

STAR★METHODS

KEY RESOURCES TABLE

REAGENT or RESOURCE	SOURCE	IDENTIFIER
Antibodies		
Bcl-xL	Cell Signaling Technology	Cat# 2764; RRID: AB_2228008
Bcl-2	Cell Signaling Technology	Cat# 15071; RRID: AB_2744528
Mcl-1	Cell Signaling Technology	Cat# 39224; RRID: AB_2799149
STAT3	Cell Signaling Technology	Cat# 12640; RRID: AB_2629499
Phospho-STAT3 (Tyr705)	Cell Signaling Technology	Cat# 9145; RRID: AB_2491009
STAT5	Cell Signaling Technology	Cat# 9363; RRID: AB_2196923
Phospho-STAT5 (Tyr694)	Cell Signaling Technology	Cat# 4322; RRID: AB_10544692
VHL	Cell Signaling Technology	Cat# 68547; RRID: AB_2716279
PARP	Cell Signaling Technology	Cat# 9532; RRID: AB_659884
cleaved PARP	Cell Signaling Technology	Cat# 5625; RRID: AB_10699459
caspase3	Cell Signaling Technology	Cat# 9662; RRID: AB_331439
cleaved caspase3	Cell Signaling Technology	Cat# 9664; RRID: AB_2070042
β-actin	Cell Signaling Technology	Cat# 12620; RRID: AB_2797972
β-tubulin	Cell Signaling Technology	Cat# 5346; RRID: AB_1950376
Chemicals, peptides, and recombinant proteins		
ABT-263	Selleck	S1001
ABT-199	Selleck	S8048
A-1331852	Selleck	S7801
A-1155463	Selleck	S7800
S63845	Selleck	S8383
Oxaliplatin	Selleck	S1224
Etoposide	Selleck	S1225
L-Asp	MedChemExpress	HY-P1923
Ruxolitinib	MedChemExpress	HY-50856
Upadacitinib	MedChemExpress	HY-19569
Fedratinib	MedChemExpress	HY-10409
PF-06651600	MedChemExpress	HY-100754
Gemcitabine	MedChemExpress	HY-17026
D-Luciferin potassium salt	Perkin-Elmer	#122799
PrimeScript™RT reagent Kit with gDNA Erase	Takara Biomedical Technology	Cat# RR047A
PowerUp™ SYBR™ Green Master Mix	Thermo Scientific Inc	A25779
Trizol	Invitrogen	Cat# 15596-026
Collagenase V	Sigma-Aldrich	Cat# C9263
DNase I	Sigma-Aldrich	#10104159001
Red Blood Cell Lysis Solution	Sangon Biotech	Cat# B541001
Cocktails	Merck	Cat# 539134
Critical commercial assays		
AnnexinV-PI apoptosis detection kit	BD Pharmingen	#556547
Bradford assay kit	Thermo Scientific Inc	Cat# 23246
P3 Primary Cell 4D X Kit	Lonza	V4XP-3032

(*Continued on next page*)

Continued

REAGENT or RESOURCE	SOURCE	IDENTIFIER
CCK-8 assay	Dojindo Molecular Technologies	# CK04
Experimental models: Cell lines		
SNK-1	Tokyo Medical and Dental University	N/A
SNK-6	Tokyo Medical and Dental University	N/A
SNT-8	Tokyo Medical and Dental University	N/A
LY	Jiang Biao's laboratory, Shanghaitech University	N/A
Experimental models: Organisms/strains		
Mouse:6 week-old Male NCG mice: NOD/ShiLtJGpt-Prkdc^{em26Cd52}Il2rg^{em26Cd22}/Gpt	GemPharmatech	NO. T001475
Oligonucleotides		
Si-STAT3-#1-F:GCUAUCUCAUCUAUGUGUU	GenePharma	N/A
Si-STAT3-#1-R:AACACAUAGAUGAGAUAGC	GenePharma	N/A
Si-STAT3-#2-F:GCUUUAGUGACUCAGAAAU	GenePharma	N/A
Si-STAT3-#2-R:AUUUCUGAGUCACUAAAGC	GenePharma	N/A
Si-STAT5A-#1-F:GCCAUAUAUUGUACAAUGA	GenePharma	N/A
Si-STAT5A-#1-R:UCAUUGUACAAUAUAUGGC	GenePharma	N/A
Si-STAT5A-#2-F:GAAUAUGUCCCUGAAACGA	GenePharma	N/A
Si-STAT5A-#2-R:UCGUUUCAGGGACAUAUUC	GenePharma	N/A
Si-Bcl-xL-#1-F:AGAGCUUUGAACAGGUAGU	GenePharma	N/A
Si-Bcl-xL-#1-R:UCUCGAAACUUGUCCAUCATT	GenePharma	N/A
Si-Bcl-xL-#2-F:GUGGAACUCUAUGGGAACA	GenePharma	N/A
Si-Bcl-xL-#2-R:CACCUUGAGAUACCCUUGU	GenePharma	N/A
Si-Screamer-F:GCATCAAGATAAGATCAAA	GenePharma	N/A
Si-Screamer-R:CGTAGTTCTATTCTAGTTT	GenePharma	N/A
RT-qPCR STAT3-F:ATCACGCCTTCTACAGACTGC	Tsingke Biotechnology Co., Ltd.	N/A
RT-qPCR STAT3-R:CATCCTGGAGATTCTCTACCACT	Tsingke Biotechnology Co., Ltd.	N/A
RT-qPCR STAT5A-F:CAGTGGTTTGACGGGGTGAT	Tsingke Biotechnology Co., Ltd.	N/A
RT-qPCR STAT5A-R:GTCGTGGGCCTGTTGCTTAT	Tsingke Biotechnology Co., Ltd.	N/A
RT-qPCR Bcl-xL-F:GCTTGGATGGCCACTTACCT	Tsingke Biotechnology Co., Ltd.	N/A
RT-qPCR Bcl-xL-R:CGACTGAAGAGTGAGCCCAG	Tsingke Biotechnology Co., Ltd.	N/A
RT-qPCR Bcl-2-F:GAACTGGGGGAGGATTGTGG	Tsingke Biotechnology Co., Ltd.	N/A
RT-qPCR Bcl-2-R:GCCGGTTCAGGTACTCAGTC	Tsingke Biotechnology Co., Ltd.	N/A

(*Continued on next page*)

Continued

REAGENT or RESOURCE	SOURCE	IDENTIFIER
RT-qPCR Mcl-1-F:AACGCGGTAATCGGACTCAA	Tsingke Biotechnology Co., Ltd.	N/A
RT-qPCR Mcl-1-R:AACGCGGTAATCGGACTCAA	Tsingke Biotechnology Co., Ltd.	N/A
RT-qPCR BFL1-F:TTGTGTCCGTAGACACTGCC	Tsingke Biotechnology Co., Ltd.	N/A
RT-qPCR BFL1-R:GGGGCAATTTGCTGTCGTAG	Tsingke Biotechnology Co., Ltd.	N/A
RT-qPCR BCL-W-F:GGCGGAGTTCACAGCTCTAT	Tsingke Biotechnology Co., Ltd.	N/A
RT-qPCR BCL-W-R:GGCGGAGTTCACAGCTCTAT	Tsingke Biotechnology Co., Ltd.	N/A
RT-qPCR β-Actin-F:GGATTCCTATGTGGGCGACGA	Tsingke Biotechnology Co., Ltd.	N/A
RT-qPCR β-Actin-R:GCGTACAGGGATAGCACAGC	Tsingke Biotechnology Co., Ltd.	N/A
Software and algorithms		
CalcuSyn	N/A	N/A
GraphPad Prism	Graphpad	N/A
CytoFLEX	Beckman	N/A
Other		
Human CD56 MicroBeads	Miltenyi Biotech	#130-050-401

RESOURCE AVAILABILITY

Lead contact

Further information and requests for resources and reagents should be directed to and will be fulfilled by the lead contact, Qianqian Yin (yinqq@shanghaitech.edu.cn).

Materials availability

This study did not generate new unique reagents.

Data and code availability

- All data reported in this paper will be shared by the lead contact upon request.
- This paper does not report any original code.
- Any additional information required to reanalyze the data reported in this paper is available from the lead contact upon request.

EXPERIMENTAL MODEL AND STUDY PARTICIPANT DETAILS

Cell lines and cell culture

SNK-1, SNK-6, and SNT-8 were kindly provided by Dr. Norio Shimizu of Tokyo Medical and Dental University and were cultured in RPMI-1640 medium (Gibco) supplemented with 10% fetal bovine serum (FBS, Gibco) and 700 U/mL interleukin-2 (IL-2, Shanghai Huaxin High Biotec). Human malignant cell lines, including NB4, U937, Jurkat, OCI-AML-3, Ramos, Raji, RS4; 11, Namalwa, SU-DHL-4, Dudi, Molt-4, HCI-H23, T-47D, Capan-1, A549, SW620, and MDA-MB-231, as well as human non-tumorigenic cells including RWPE-1, HFF-1, and HL-7702, were obtained from ATCC and the Shanghai Cell Bank of the National Science Academy of China (Shanghai). GES-1 cells were obtained from Cancer Hospital Chinese Academy of Medical Sciences. Nasopharyngeal carcinoma cells were obtained from Sun Yat-sen University Cancer Center. All cell lines were cultured according to the provider's instructions in a humidified incubator at 37°C and 5% CO2/95% air (v/v) and were routinely

checked and negative for mycoplasma contamination as assessed by the MycoAlert Mycoplasma Detection Kit (Lonza).

Animals

All animal experiments were conducted at the Laboratory Animal Center at the National Centerfor Protein Science Shanghai. All experimental protocols for the procedures with animals were approved by the committee for the humane treatment of animals at Shanghai Tech University and Shanghai Jiao Tong University School of Medicine (IACUC approval # 20201026001). 4–6 weeks male NCG mice (NOD/ShiLtJGpt-Prkdc^{em26Cd52}Il2rg^{em26Cd22}/Gpt, Strain NO.T001475) weighing approximately 18–20 g of were purchased from the GemPharmatech and maintained in an SPF animal housing facility. Mice had access to food and water *ad libitum* and were kept at a constant temperature on a 12-h light/dark cycle.

Human subjects

The cohort consists of 91 patients with pathologically confirmed ENKTL at Xinhua Hospital Affiliated to Shanghai Jiao Tong University School of Medicine from January 2017 to January 2021, including 21 patients from other hospitals who underwent pathology consultation at Xinhua Hospital and were excluded from the survival analysis due to the lack of follow-up. Informed consent was obtained from all patients in accordance with the Declaration of Helsinki, and all manipulations were approved by the Medical Science Ethic Committee of Xinhua Hospital, Shanghai Jiao Tong University School of Medicine (permission No. XHEC-D-2018-006). After ethical approval, tumor samples and specimens were obtained. The detailed clinical and pathological information including age, gender, clinical stages and IHC score in this study were listed in Table S2.

METHOD DETAILS

Primary cell isolation

PBMCs (peripheral blood mononuclear cells) obtained from six healthy adult donors were purchased from Shanghai Miao-tong Biological Technology (PB009C-1, HemaCare). In addition, the human primary CD56$^+$ NK cells were enriched and purified from PBMCs of one healthy adult donor using miniMACS (Magnetic cell selection) and human CD56 MicroBeads (130-050-401, Miltenyi Biotech) following the manufacturer's instructions. The xenograft mice were euthanized by CO_2 inhalation at humane endpoint. Once euthanasia was performed, collection of tissues was initiated immediately and was complete within 3 min. Spleens were removed from PDX mice and were homogenized into a single-cell suspension using PBS supplemented with 2% FBS. The single-cell suspension of bone marrow derived from PDX mice was prepared by keeping flushing the bones with PBS till the bones' color turned from red to white. The tumor pieces or infiltrated tissue (i.e., kidney) pieces of xenograft mice were substantially minced into small pieces and then digested with an enzyme mixture with collagenase V (1 mg/mL, cat# C9263, Sigma-Aldrich) and DNase I (1 mg/mL, 10104159001, Sigma-Aldrich) at 37°C. Red blood cells were then lysed by resuspending cells in Red Blood Cell Lysis Solution (cat# B541001, Sangon Biotech, Shanghai). The cell suspensions were filtrated through a 70 μm strainer to remove cell aggregates and cell viability was determined.

High throughput compound screening

The chemical compound library used for screening consisted of 2,076 FDA-approved drugs and bioactive products. Compounds were dissolved in DMSO in StorPlate-384V (PerkinElmer) and added into 384-well plates (Thermo) pre-seeding with SNK-6 cells (2×10^5/mL, 60 μL/well) at a final concentration of 1 μM (0.1% DMSO) through the Agilent Bravo liquid handling platform. The wells were incubated at 37°C, 5% CO2 for 48 h, and cell growth was detected utilizing the CCK-8 assay (CK04, Dojindo Molecular Technologies, MD) by reading the absorbance at 450 nm in a microporous plate detection system (PerkinElmer Envision, California). In each 384-well assay plate, 24 wells were used as the positive control (0.1% DMSO with 1 μM Gemcitabine), 24 wells as the negative control (0.1% DMSO without any compounds), and 16 wells as blank control. Compounds showing greater than 50% inhibition relative to negative controls were considered "hits". The drug screening results are included in Table S1.

Cell growth inhibition

2×10^5/mL cells were seeded into a 96-well or 384-well tissue culture plate. Then compounds were 2-fold serially diluted in the corresponding medium into each well. Cells were incubated for 48 h, and cell growth was evaluated utilizing the CCK-8 assay. The readings were normalized to the DMSO-treated cells and

fitted using a nonlinear regression analysis with the GraphPad Prism 8 software to obtain the IC_{50} value for each compound.

Cell apoptosis

Cells were seeded in 12-well plates and treated with the indicated treatments for 24–48 h. The apoptosis assays were conducted using the AnnexinV-PI apoptosis detection kit (556547, BD Pharmingen) and analyzed by the CytoFLEX (Beckman Coulter).

Immunohistochemistry

Immunohistochemical staining was performed on a Dako Omnis Autostainer (Dako, Agilent Technologies Inc.) according to the manufacturer's instructions. Briefly, sections were baked at 60°C for 30 min and then loaded onto the Dako Omnis Autostainer for deparaffinization, antigen retrieval, antibody incubation, and detection. Antigen retrieval was performed using EnVision FLEX Target Retrieval Solution, high pH at 97°C for 30 min. The primary antibody (1:200 dilution, CST) was incubated at room temperature or 4°C. Detection was performed using the EnVision FLEX/HRP reagent for 30 min. The IHC staining of positive and negative controls was performed to determine the specificity of the observed antibody staining. Positive control issues included breast cancer tissue (for Bcl-2, Mcl-1), lung cancer tissue (for Bcl-xL), rectal cancer tissue (for BCL-W), and colon cancer tissue (for BFL1). Negative controls included: the mouse isotype control (for Bcl-2) and the rabbit isotype control (for Bcl-xL, Mcl-1, BCL-W, and BFL1). For the quantitative analysis, the H-score was calculated based on the staining intensity and percentage of stained cells. The intensity score was defined as follows: 0, negative; 1, weak staining; 2, intermediate staining; 3, strong staining. The fraction of positive cells was scored as 0–100%. The H-score was calculated by multiplying the intensity and fraction scores, producing a total range of 0–300. The optimal cutoff point for the definition of Bcl-xL high/low expression subgroups was calculated. Patient cases exhibiting an H-score (<180) were pooled in the Bcl-xL low expression group, whereas patients with a higher H-score ($\geq$ 180) were designated Bcl-xL high expression group.

Western blotting

2×10^5 cells/mL were plated in 6-well plates and treated with compounds as indicated. Cells were collected, washed with cold 1 × PBS, and lysed in 1 × SDS buffer containing protease inhibitor cocktails (cat.539134, Merck). Protein in cell lysate was quantified by detergent-compatible Bradford assay kit (cat.23246, Thermo). The Millipore immobilon Western chemiluminescence substrate was used for signal development. Blots were imaged in an Amersham Imager 600 (G.E. Healthcare).

Quantitative real-time PCR

Total RNA was extracted using Trizol (cat.15596-026, Invitrogen) and reverse transcribed into cDNA using the PrimeScript RT reagent Kit with gDNA Eraser (Perfect Real Time) (cat. RR047A, Takara Biomedical Technology). Real-time PCR was performed using PowerUp SYBR Green Master Mix (Thermo Scientific Inc). Melting curve analysis was performed to ensure amplification specificity. Relative gene expression was calculated using the 2-ΔΔCt method. Primers used for qPCR are as follows.

RNA interference

SNK-6 and LY cells (5×10^5 cells) were nucleofected with 50 pmol of each target siRNA duplex using Amaxa P3 Primary Cell for 4D-Nucleofector X Kit S (cat. V4XP-3032, Lonza) according to the manufacturer's protocol. Then cells were incubated for 24–48 h and collected for future analysis.

Short tandem repeat (STR) analysis

STR analysis was performed using PowerPlex 18D system (Promega Corporation) according to the manufacturer's instructions. DNA extracted from tumor tissues was amplified by multiplex PCR for 21 loci, including 20 STR loci -D13S317, D18S51, D19S433, D21S11, D3S1358, D7S820, D8S1179, D16S539, D2S1338, D5S818, D1S1656, D6S1043, D12S391, fibrinogen α chain (FGA), Penta E, Penta D, von Willebrand factor type A (vWA), THO1, TPOX, CSF1PO, and amelogenin. Primers and DNA polymerase were included in the kit (cat. no. DC1802; Promega Corporation). The internal lane standard was labeled with the dye WEN (included in the kit). PCR products were electrophoresed on an ABI 3130×L Genetic Analyzer (Applied Biosystems; Thermo Fisher Scientific, Inc.) and analyzed with GeneMapper 4.0 software (Thermo Fisher Scientific, Inc.) using allelic ladders supplied by Applied Biosystems (Thermo Fisher Scientific, Inc.). The SRT analysis results in tumor tissues from the two PDX models and the corresponding original patient are in Table S4.

Establishment and analysis of CDX xenograft model

SNK-6 cells stably transfected with luciferase reporter (termed SNK6-Luc) were intraperitoneal (i.p.) injected into highly immune-deficient NCG mice, and human recombinant IL-2 was also administered to support the cell proliferation *in vivo* according to the previously reported procedure.[29] Two weeks after transplantation, SNK6-Luc tumor-bearing NCG mice were grouped according to the bioluminescence value using a Xenogen IVIS imaging system. NCG mice were treated with vehicle, ABT-263, ABT-199, and A-1331852 at indicated doses for two weeks ($n \geq 6$ for each group) and were observed for at least another week after drug withdrawal. ABT-263 and ABT-199 were administrated consecutively for 14 days, and A-1331852 was given for five consecutive days, followed by two days of rest per week. Drugs were formulated in DMSO/Cremophor EL/saline (1:2:7, v/v). The tumor growth was measured through bioluminescence following an intravenous injection of 150 mg/kg (15 mg/mL in PBS) D-luciferin (cat.122799, PerkinElmer Envision, California) after anesthesia for a short period of time (30 s–1 min) in a sealed chamber containing the inhalation anesthetic isoflurane. The peripheral blood cells were collected from the tail using a capillary tube after anesthesia with isoflurane for platelet count analysis. Apply pressure or use a cauterizing agent to stop the bleeding. Tumor-bearing mice were euthanized by CO_2 inhalation conformed to the following termination criteria: when the tumor volume reached 10% of net body weight, or the tumor size exceeded 1.5 cm in diameter, or when the animals became moribund with severe weight loss (>15%), or mice showed signs of distress. The mice were placed in a transparent box that released pure CO_2 at the defined humane endpoint. When mice were observed to faint, CO_2 continued to be released for 2 mins for euthanization. The tumor section was isolated for H&E and immunohistochemical staining of human Ki-67 and cleaved caspase-3 in tumor sections of drug-treated mice following the continuous daily treatment for four days. All animal handling was approved by the committee for the humane treatment of animals at Shanghai Tech University and Shanghai Jiao Tong University School of Medicine (IACUC approval # 20201026001).

Establishment and analysis of PDX xenograft models

Surgical tumor samples used for PDX mice were obtained from two relapsed and refractory ENKTL patients from Xinhua Hospital of Shanghai Jiao Tong University School of Medicine in accordance with the Declaration of Helsinki, and were approved by the Medical Science Ethic Committee of Xinhua Hospital, Shanghai Jiao Tong University School of Medicine (permission No. XHEC-D-2018-006). Tumor cells for PDX -#1 were obtained from a patient with relapsed/refractory ENKTL failing radiotherapy, L-asparaginase-based regimens (P-Gemox, MEDA), and anti-PD1 antibody (Tislelizumab), the disease relapsed with nasopharyngeal, skin, and bone marrow involvement. The skin lesion biopsy was collected at the stage of disease progression after the last line of PD-1 mAb therapy. Tumor cells for PDX-#2 were obtained from a relapsed ENKTL patient following treatment with CHOP+RT (cyclophosphamide, doxorubicin, vincristine, and prednisone plus radiotherapy), L-asparaginase-based regimens (P-Gemox, MEDA), and anti-PD1 antibody (Tislelizumab), the disease relapsed with skin of lower limbs, muscle, spleen, and lymph node involvement. The skin lesion biopsy was collected at the stage of disease progression after the last line of PD-1 mAb therapy. In brief, surgically removed tumor tissues (P0) were cut into fragments of ~15 mm^3 and implanted using a trocar needle subcutaneously into male NCG mice (6–8 weeks) within 2 h for engraftment (P1). The PDX mice were given an intraperitoneal injection of human recombinant IL-2 to support engraftment according to the procedure described in the SNK-6 xenograft model above. When the PDX-P1 mice exhibited such rough fur, decreased physical activity, a faster breathing rate, and apparent weight loss, the disease occurred. Then the PDX mice were euthanized by CO_2 inhalation conformed to the following termination criteria: when the tumor volume exceeded 1000 mm^3, or the tumor size exceeded 1.5 cm in diameter, or when the animals became moribund with severe weight loss (>15%), or mice showed signs of distress. The mice were placed in a transparent box that released pure CO_2 when reaching the defined humane endpoint. When mice were observed to faint, CO_2 continued to be released for 2 mins for euthanization. The tumor pieces or infiltrated tissue were dissected and the xenografts were transferred by serially passaging to secondary recipient NCG mice. The transplantation of tumor cells from the isolated single-cell suspension of spleen cells (i.v.; 2×10^6 cells/mouse) of P1 PDX mice was performed to passage to secondary recipient NCG mice (P2). The *in vivo* efficacy of BH3-mimetic drugs of Bcl-2 family members was performed on day 7 after engraftment in P2 passage of PDX mice according to the administration protocols in the SNK-6 xenograft model. The mice were euthanized by CO_2 inhalation conformed to the above euthanization criteria. The survival time of each mouse was recorded and the tumor pieces or infiltrated tissue were dissected for future analysis. All animal handling was approved by the committee for the humane treatment of animals at Shanghai Tech University and Shanghai Jiao Tong University School of Medicine (IACUC approval # 20201026001).

Establishment and characterization of LY cells

The novel ENKTL cell line LY was established from PDX-#1 murine model. After two PDX passages, separation of $CD56^+$ cells were performed by positive selection cell sorting methods utilizing anti-human CD56 antibody-based magnetic beads (MACS, Miltenyi Biotec) from splenic mononuclear cells of the PDX-#1 murine model (anti-human $CD56^+$ population: 73.4% before MACS isolation versus 94.58% after MACS isolation). The purified $CD56^+$ cells were subjected to cell culturing under the same culture conditions as SNK-6 cells in the supply of human recombinant IL-2 until the cells constantly doubled their number within 24 h. The detailed information is shown in Figure S1. The morphology of LY cell cells is similar to that of SNK-6 cells, exerting several cell clumps in suspension and medium to large cell size with large nuclei and abundant cytoplasm. Cell-surface marker analysis by flow cytometry revealed that LY cells are $HLA\text{-}DR^+CD3^-CD16^-CD56^+$, indicating an NK phenotype. Finally, the STR patterns of the LY cells did not match those of any cell lines in the public cell banks, such as the ATCC, DSMZ, or JRCB, and did not contaminate with murine cells. Hence it is concluded that LY is a new ENKTL cell line.

Synergy calculations

The combination index (CI) values and Fraction (Fa) values for the drug combination at a constant ratio were calculated using CalcuSyn software. $CI < 1$ indicates synergism; $CI = 1$ indicates additivity; $CI > 1$ indicates antagonism.

QUANTIFICATION AND STATISTICAL ANALYSIS

The data are presented as the mean $\pm$ SD and n represents the number of biological replicates, unless otherwise stated. All cellular experiments consisted of a minimum of three independent replicates and were repeated at least three times. Statistical tests were performed using Microsoft Excel and GraphPad Prism Software version 8.0. For comparisons of the two groups, a two-tailed unpaired t-test was used. For comparisons of multiple groups, a one-way ANOVA analysis of variance was used. A Log rank test was performed for survival curves. The levels of significance were set at $p < 0.05$ (*), $p < 0.01$ (**), and $p < 0.001$ (***). Details for each figure are included in the Figure Legends.

ADDITIONAL RESOURCES

The clinical Trial has been registered on ClinicalTrials.gov (Identifier: NCT05186012, URL: https://clinicaltrials.gov/ct2/show/NCT05186012).